# CCI

# BIOMASS

# PRODUCT VALIDATION & INTERCOMPARISON REPORT

# YEAR 2

# VERSION 2.0

| | |
|---|---|
| DOCUMENT REF: | CCI_BIOMASS_PVIR_V2.0 |
| DELIVERABLE REF: | D4.1_PVIR |
| VERSION: | 2.0 |
| CREATION DATE: | 2020-12-17 |
| LAST MODIFIED | 2020-12-17 |

Document Authorship

| | NAME | FUNCTION | ORGANISATION | SIGNATURE | DATE |
|---|---|---|---|---|---|
| PREPARED | S. de Bruin | WP7 | Wageningen University | | |
| PREPARED | A. Araza | WP7 | Wageningen University | | |
| PREPARED | M. Herold | WP7 Lead | Wageningen University | | |
| PREPARED | | | | | |
| PREPARED | | | | | |
| PREPARED | | | | | |
| PREPARED | | | | | |
| PREPARED | | | | | |
| PREPARED | H. Kay | A. Project Manager | Aberystwyth University | | |
| PREPARED | R. Lucas | Project Manager | Aberystwyth University | | |
| VERIFIED | S. Quegan | Science Leader | Sheffield University | | |
| APPROVED | | | | | |

Document Distribution

| ORGANISATION | NAME | QUANTITY |
|---|---|---|
| ESA | Frank Seifert | |

Document History

| VERSION | DATE | DESCRIPTION | APPROVED |
|---|---|---|---|
| 0.1 | 2019-12-18 | First draft version | |
| 1.0 | 2019-12-18 | | |

Document Change Record (from Year 1 to Year 2)

| VERSION | DATE | DESCRIPTION | APPROVED |
|---|---|---|---|
| 2.0 | 2020-12-17 | Finalised version 2.0 | |
| | | | |

# TABLE OF CONTENTS

# LIST OF TABLES

# LIST OF FIGURES

# SYMBOLS AND ACRONYMS

| | |
|---|---|
| AGB | Aboveground biomass |
| $AGB_{map}$ | Aboveground biomass according to the map |
| $AGB_{ref}$ | Aboveground biomass from plot, corrected for plot inventory date and if plot size < 1 ha, corrected for partial forest fraction at pixel level |
| CCI | Climate Change Initiative |
| CoFor | Congo basin Forests AGB dataset (Ploton et al., 2020) |
| GNSS | Global Navigation Satellite System |
| IPCC | Intergovernmental Panel on Clmate Change |
| $I_{Var}$ | Indicator variable: 1 if the $SE_{CCI}$ is consistent with $Var(Plt)$, MD and MSD, and 0 otherwise. The latter indicates that the $SE_{CCI}$ layer is overly pessimistic regarding AGB map precision. |
| LiDAR | LIght Detection And Ranging |
| MD | Mean difference between $AGB_{map}$ and $AGB_{ref}$ |
| MSD | Mean square difference (between $AGB_{map}$ and $AGB_{ref}$) |
| NEON | National Ecological Observatory Network, USA |
| NFI | National Forest Inventory |
| PUG | Product User Guide (Santoro, 2020) |
| PVIR | Product Validation and Inter-comparison Report |
| PVP | CCI Biomass Product Validation Plan |
| RMSD | Root mean square difference (between $AGB_{map}$ and $AGB_{ref}$) |
| $SE_{CCI}$ | Error layer (standard deviation) provided with the CCI Biomass product; if squared denoted as $SE^2_{CCI}$. |
| SLB | Sustainable Landscape Brazil |
| SRTM | Shuttle Radar Topography Mission |
| TERN | Terrestrial Ecosystem Research Network, Australia |
| Var(Plt) | Estimated variance of the plot measurement error |
| Var(S(x)) | Estimated variance of the within-pixel sampling error (owing to smaller plot footprint) |

# 1. Introduction

Validation is critical for raising acceptance of satellite-derived products in the user community. To assess the accuracy of the aboveground biomass (AGB; Mg/ha) estimates of the epochs 2017, 2018 and the refined 2010 CCI Biomass global products (Santoro, 2020), AGB predictions from the map have been compared with independent AGB data from plots and LiDAR campaigns, which were used as reference values. The main aim of this report is to provide an independent assessment of the quality of the three CCI Biomass products, with this primarily providing (climate) users with uncertainty information when using the map for global and regional climate modelling and assessment purposes. A second purpose is to provide feedback to map producers to establish where the map can be improved.

The reference AGB data are not error-free. *In situ* estimates of AGB are computed based on stem diameter (typically cm), tree height (m), wood density (g $cm^3$) and allometric models, while geolocation is determined using Global Navigation Satellite System (GNSS) measurements having variable and often limited accuracy. GNSS accuracy is degraded if the paths between the satellites and the GNSS receiver are partly blocked by vegetation cover, which is not uncommon in forests. An additional cause of discrepancies between plots and pixel-based AGB estimates is the difference in support (shape and size) between map pixels and plots. The latter are often much smaller than the pixels they are being compared with, which may introduce a spatial representation error (referred to as the within-pixel *sampling error*). This occurs, for example, if a forest plot is used to represent a pixel that is only partially forested. But even if the pixel's footprint is fully covered by forest, AGB heterogeneity inside the pixel produces differences between plot values and pixel AGB. A similar effect occurs when comparing pixel means over, for example, 0.1° cells to the mean of plots inside these blocks. Additionally, the plot inventory date often differs from the biomass map epoch, which gives a temporal mismatch between the compared AGB values.

LiDAR-based AGB estimates used as reference data can completely cover map pixels or even larger pixel blocks, which eliminates the sampling errors referred to above. However, just like the *in situ* estimates of AGB, LiDAR-based AGB values are themselves predictions, so are subject to prediction error that has to be taken into account.

Each of the above-mentioned factors can introduce errors with a random or a systematic nature. The latter type of error is of particular concern since it cannot be reduced by aggregating individual tree measurements over large plots or by averaging small plot data over many plots. Systematic errors in reference data have to be reduced as much as possible by adhering to a standardized measurement protocol (Labrière et al., 2018).

Versions 1 and 2 of the CCI Biomass Product Validation Plan (PVP; de Bruin et al., 2019a, 2020) presented approaches for addressing the temporal mismatch between plot and pixel data and partial forest fractions within map pixels. The reports also proposed methods for assessing the variance of the other error sources. In this second PVIR, the temporal mismatch between plot and pixel data and partial forest fractions within map pixel are handled similarly as in the first PVIR. The proposed approaches for accounting for other error sources are partly implemented, up to the point supported by available data.

An extensive dataset of forest plot data across the world was acquired for the purpose of the validation (see Appendix A, Figure 1 and Table 1). Like before, the plots underwent a series of quality checks (see Section 2.1). Forest plot data and LiDAR were not used to calibrate the CCI Biomass map in order to guarantee full independence from the production process. The contributions of AGB measurement error and spatial representation error are known to be largest for small plots such as National Forest Inventory (NFI) plots, while detailed measurements of all trees within large plots are deemed to deliver highest quality AGB data (Réjou-Méchain et al., 2019; Réjou-Méchain et al., 2014). To take into account expected differences in the accuracy of plot data, a tiered approach was chosen which comprised:

- Tier 1 - small plots (≤ 0.6 ha) including National Forest Inventory (NFI) data,
- Tier 2 - larger plots (0.9-3 ha; tier 2), and
- Tier 3- high-quality large super-plots (≥ 6 ha; mainly from Labrière et al. (2018).

Note that the tier numbering differs from PVIR version 1, to make it consistent with IPCC (2006) tier numbering where tier 3 is the most demanding in terms of data requirements. The tiers were analysed separately in the plot-pixel comparisons. AGB map comparisons with data derived from LiDAR and aggregated plot data (see Section 2.2) were also analysed separately.

The map inter-comparison presented in this document concerns consistency of map-reference deviations amongst the three current CCI Biomass AGB products and comparisons with the GlobBiomass 2010 AGB product (http://globbiomass.org) and version 1 of the CCI Biomass 2017 product.

# 2. Materials and methods

## 2.1. Forest plot data

For CCI Biomass, new forest inventory and plot data from research networks were added to the existing GlobBiomass reference database (Rozendaal et al., 2017). Reference data were only included if quality criteria, as described in the PVP, were met. Specifically, the plots needed:

- A proper citable reference source and metadata to assess the procedures and quality of biomass estimation.
- Precise coordinates (4-6 decimals for coordinates in decimal degrees).
- A census date within ten years from the reference year of the AGB map to avoid temporal inconsistency with the assessed maps.
- Measurements of all trees of diameter ≥ 10 cm (or less) were included.
- Not deforested between the year of the inventory and the reference year of the CCI Biomass map (i.e., 2010, 2017 and 2018). The latter assessment was based on the 2018 forest loss layer of the Hansen dataset (Hansen et al., 2013).

Table 1 lists the numbers of plots used in each tier and for each of the map reference years.

Table 1. Number of plots used in each tier for the different AGB map reference years.

| Map ref. year | tier1 | tier2 | tier3 | Total |
|---|---|---|---|---|
| 2010 | 118126 | 737 | 27 | 118853 |
| 2017 | 68286 | 557 | 23 | 68845 |
| 2018 | 65088 | 485 | 21 | 65573 |

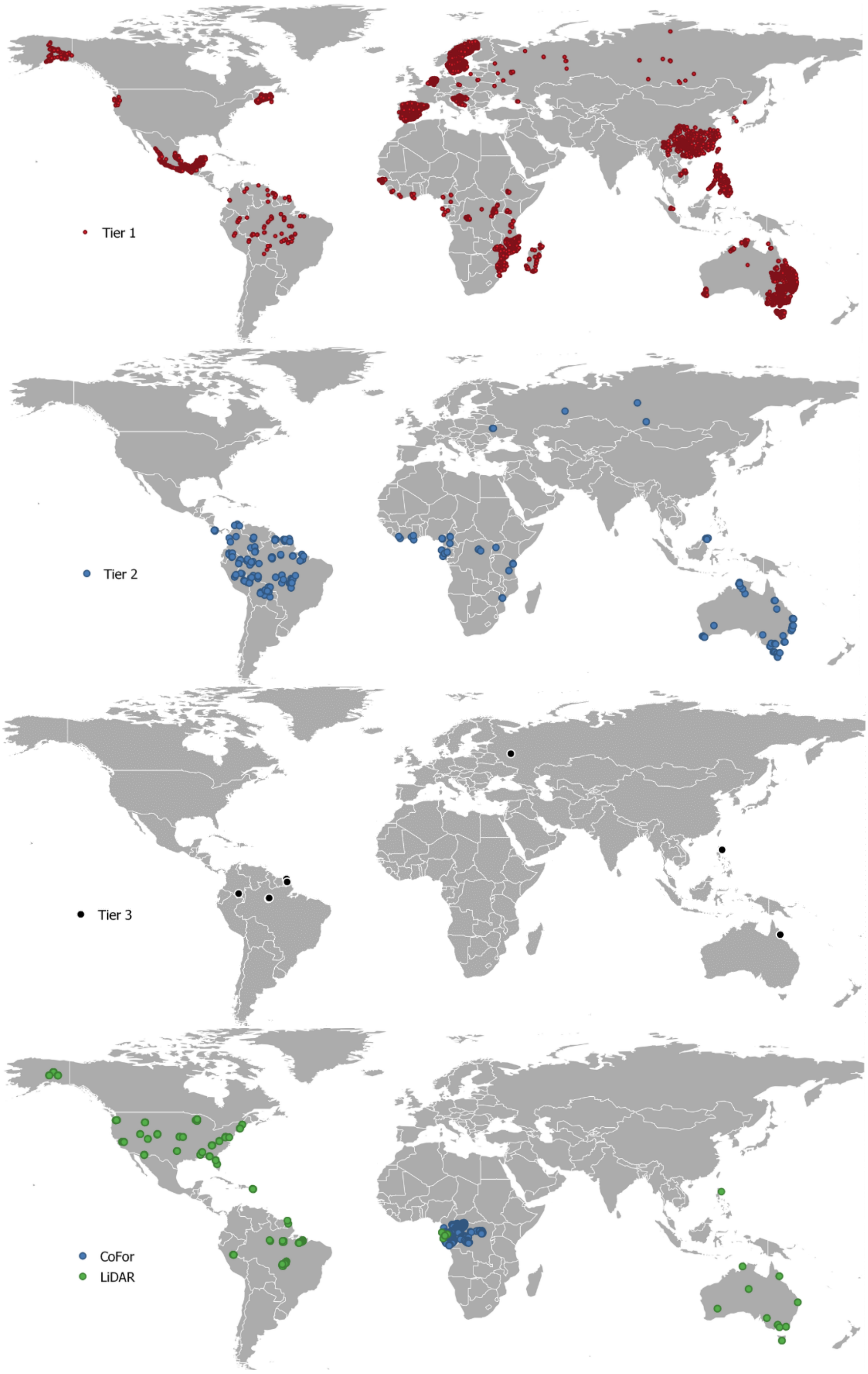


Figure 1. Geographical locations of plots and footprints (CoFor and LiDAR) of the reference datasets.

## 2.2. LiDAR-based and 1-km pixel Congo basin Forests AGB

In addition to the plot data, we used LiDAR-based AGB data at 100 m resolution from the Sustainable Landscape Brazil project (SLB), the National Ecological Observatory Network, USA (NEON) and the Terrestrial Ecosystem Research Network, Australia (TERN) processed by Labrière and Chave (2020a, b, c). The 1-km pixel forest management inventory data used in this report originate from the Congo basin Forests AGB (CoFor) dataset (Ploton et al., 2020). Concerning the latter dataset, only pixels having at least five in situ forest management inventoried plots were used.

Table 2 lists the numbers of LiDAR and CoFor footprints used in each tier and for each of the map reference years.

Table 2. Number of LiDAR and CoFor footprints used for the different AGB map reference years.

| Map ref. year | CoFor | LiDAR | Total |
| --- | --- | --- | --- |
| 2010 | 16896 | 155444 | 172340 |
| 2017 | 9356 | 1037218 | 1046574 |
| 2018 | 8777 | 1040529 | 1049306 |

As described in the PVPs, we rely on opportunistic AGB plot data that were not specifically produced for validation purposes but that are rather collected within the context of national forest inventories and research efforts at local to regional scale.

## 2.3. Preparation of validation datasets

### Temporal harmonization

Differences between the inventory date of AGB plots and the reference year of the AGB map were harmonized using updated IPCC growth rates (IPCC, 2019; Requena Suarez et al., 2019) following the approach described in Version 1 of the PVP. For plots in tropical and subtropical ecological zones, age category dependent growth rates are available (IPCC, 2019; Requena Suarez et al., 2019). In those cases, plot AGB values in the range 0-99 Mg/ha were assumed to represent young secondary forest, AGB values in the range 100-128 Mg/ha were treated as old secondary forest (Van Breugel et al., 2007), AGB above 129 Mg/ha was assumed to correspond to old growth stands (Brown et al., 1989; Clark & Clark, 2000; Mello et al., 2016). Given the absence of data on plot forest age, low biomass but mature forests could not be distinguished from young stands, with potential implications for the applied growth rates. For temperate oceanic forests in Europe and boreal coniferous forests and tundra woodlands, no differentiation of growth rates over age categories was used. The temporal adjustments by growth rates were applied up to a difference of ten years between the inventory date and the map reference year. Plots having a longer temporal difference were discarded in the analyses. The LiDAR dataset was exempted from temporal adjustment because it contained repeated measurements between 2011 and 2018.

### Correction for forest fraction

As described in the PVP, correction for inclusion of non-forested areas within map pixels was undertaken by multiplying the temporally adjusted plot AGB by forest fraction at the pixel level. This forest fraction was computed by setting a 10 % threshold on the 2010 tree cover product (Hansen et al., 2013), which had a resolution of 1 arc-second per pixel, or approximately 30 meters per pixel at the equator. In the rare case of more than one AGB plot within a pixel, the average of the adjusted AGB per plot was used. The correction for forest fraction was only applied to plots with an area below 1 ha.

### Comparisons at 0.1° cell resolution

To reduce the effect of short range AGB variations in the map and their potential interaction with plot-map geolocation mismatches and to assess the CCI Biomass map at a resolution commonly used by climate modellers, $AGB_{map}$ - $AGB_{ref}$ comparisons from tier 1 data were also made over multi-pixel blocks at 0.1° cell resolution. In this case, correction for partial forest fraction (see above) was undertaken at the level of the coarse resolution cells. Mean $AGB_{ref}$ at 0.1° cell level was computed by multiplying forest fraction at the 0.1° cell level by the mean temporally adjusted AGB of at least five plots in that cell. The procedure is illustrated in Figure 5 of the PVP (de Bruin et al., 2019a). The AGB reference values thus obtained were compared with the average map AGB spatially aggregated over the 0.1° cells.

The correction for forest fraction was not applied to the LiDAR dataset since the LiDAR footprints were assumed to representatively sample forest/non-forest fractions within the 0.1° cells, i.e., forested areas were not preferentially sampled.

### Ecoregions / biomes

$AGB_{map}$ - $AGB_{ref}$ comparisons at 0.1° cell resolution were also stratified according to ecoregions derived from the recent global ecoregion map (Dinerstein et al., 2017), which was downloaded from https://ecoregions2017.appspot.com/. The original vector maps were rasterized to 0.1° resolution. Resulting raster cells were assigned to the category covering the largest portion of the cell area. We stratified comparisons from tier 3 data at 0.1° cell resolution per biome.

## 2.4. Comparing AGB map pixels with reference data

### Assumptions

After adjustments for temporal discrepancies and partial forest fraction and having at least ten plots within a reference biomass range, we assumed unweighted means computed from reference data in tiers 1 and 2 to be unbiased. The biomass ranges used are listed in the first column of Table 2. For tier 1 data, we relaxed the requirement of ten plots per biomass range because these data were recorded over large plots (≥ 6 ha) and followed a strict measurement protocol. Under the unbiasedness assumption, mean differences between harmonized plot data and map values aggregated over bins covering ranges of reference AGB values are interpreted as *map bias*. To empirically verify the assumption of unbiased plot data, we conducted the analyses for each of the three tiers and assessed consistency of results over the three tiers, whenever data volume allowed us to do so.

When reporting mean differences (MD) and (root) mean square difference ((R)MSD) over ecoregions, we assume that plot-map comparisons within ecoregions are representative of those regions.

To facilitate a preliminary assessment of the standard deviation layer accompanying the CCI Biomass maps (see below), we assumed map error and plot measurement error to be spatially uncorrelated and mutually uncorrelated. This assumption was made because, at the time of writing this report, we had only limited data for assessing spatial correlation structures of the error components see sections 2.5 and 2.6).

### Measures

Besides reporting mean differences between reference and map AGB per biomass range, which are interpreted as map bias (see above), we also report (root) mean square deviations (MSD) between map values and plots. At this stage, we did not interpret MSD as the mean square *errors* of the map since we will elaborate on the assessment of the variance of individual error components in later stages of the project. However, we did assess whether the mean variance of map error ($mean(SE_{CCI}^2)$)—where $SE_{CCI}$ is the standard error layer provided with the CCI Biomass map—is consistent with *MSD*, *MD* and the mean variance of plot measurement error $mean(Var(Plt))$. The $SE_{CCI}$ layer only represents the random part of AGB errors (Santoro, personal communication). Leaving out three random error components listed in the PVP (positional error, within-pixel representation error and the data harmonization error) and under the assumptions given above, we checked whether

$$mean(SE_{CCI}^2) \leq MSD - MD^2 - mean(Var(Plt)).$$

For this purpose, we defined an indicator variable $I_{Var}$, as follows:

$$I_{Var} = \begin{cases} 1 \;\; if \; mean(SE_{CCI}^2) \leq MSD - MD^2 - mean(Var(Plt)) \\ \qquad\qquad\qquad 0 \;\; otherwise \end{cases}$$

If $I_{Var}$ attains the value zero, $mean(SE_{CCI}^2)$ would be too large or—in other words—the $SE_{CCI}$ layer provided with the biomass product would be overly pessimistic about map precision, unless the variance of plot measurement error is greatly underestimated.

For plots having tree-level data, $Var(Plt)$ was computed using the Réjou-Méchain et al. (2017) biomass R-package. For other plots lacking such data, $Var(Plt)$ was predicted by a random forest model trained on the plots having tree-level data, using plot biomass, plot size, general and specific eco-zones and continent as explanatory variables.

## 2.5. Spatial correlation of AGB

Experimental semi-variograms were computed and variogram models were fitted using gstat (Pebesma, 2004) based on LiDAR-AGB data acquired over two forest sites in Remningstorp, Sweden, and Lope, Gabon, i.e., a *boreal* and a *tropical* forest site. These ALS datasets were acquired in the framework of the airborne ESA BIOSAR (Ulander et al., 2011) and AfriSAR (Hajnsek et al., 2017) campaigns to provide detailed information on forest vertical structure and to produce high-resolution AGB maps. The AGB data have a spatial resolution of 10 m (Remningstorp) and 20 m (Lope) and were also used in version 2 of the Product User Guide (PUG; Santoro, 2020). Non-forest areas (such as savanna in the Lope study area) were masked out after manually digitizing forested areas using high resolution Google Earth imagery. Accordingly, the variogram models represent spatial correlation of AGB within forested area at the study sites.

## 2.6. Effect spatial support on sampling error and suggested map bias

The variogram models described above were used to assess the effects of the within-pixel sampling error (see Introduction) for the forest sites in Remningstorp and Lope. This was undertaken through two means:

- By computing the variance of the difference between sub-pixel plots and plot configurations (i.e., for plots smaller than pixels) and AGB map pixels at locations $x$ as:

$$\begin{aligned} Var\big(S(x)\big) &= Var\left(AGB_{ref}(x) - AGB_{map}(x)\right) \\ &= Var\big(AGB_{ref}\big) + Var\big(AGB_{map}\big) - 2 * Cov\big(AGB_{ref}, AGB_{map}\big), \end{aligned}$$

  where $Var\big(AGB_{ref}\big)$ is the sill of the variogram at the spatial support of the plots, $Var\big(AGB_{map}\big)$ is the within pixel covariance, and $Cov\big(AGB_{ref},\ AGB_{map}\big)$ is the plot to pixel covariance. Note that for brevity reference to the location x is omitted at the right-hand side of the above equation. The latter two terms are computed using the geostatistical framework of change of support (Kyriakidis, 2010).

- By simulating possible plot AGB, conditional on given AGB values at the pixel level, using the $Var\big(AGB_{ref} - AGB_{map}\big)$ computed in the above step. The aim of this simulation is to reproduce and explain results in section 3.3 of the PUG (Santoro, 2020) by a geostatistical approach.

# 3. Validation results for the global maps

## 3.1. Global assessments per tier of plot data

### Tier 1 non-aggregated

The non-aggregated results (i.e., at original resolution) of global plot-map comparisons using tier 1 data (plot size ≤ 0.6 ha) are shown in Figure 2 and Tables 3-5.

An overall feature of the comparisons is over-prediction of low reference biomass and under-prediction of higher reference biomass values, while relative accuracy is within 20 % in the middle range. On average, under-prediction by the map starts occurring at a reference biomass of approximately 150 Mg/ha but the interquartile range of plot data still covers the 1:1 line between $AGB_{ref}$ and $AGB_{map}$ up to approximately 275 Mg/ha. The under-prediction increases with reference biomass and reaches maxima of 489 Mg/ha (2010), 481 Mg/ha (2017) and 474 (2018) for mean reference biomass densities of 782, 785 and 783 Mg/ha, respectively. The latter values originate from small plots with exceptionally high biomass that are unlikely to cover extensive areas and are unlikely to be captured by the biomass retrieval algorithm. The banding observed in the left column of Figure 2 seems to be caused by a maximum AGB level set for particular regions in the retrieval algorithm. Upon a first impression, the accuracy of the 2017 map has improved with respect to the previous edition as reported in de Bruin et al. (2019b: Table 4 and Figure 4 therein). This is further analysed in section 3.7.

As noted in the PUG (Santoro, 2020), the within-pixel sampling error contributes to the observed over-prediction of low reference biomass and under-prediction of higher reference biomass values, even if the mean AGB of the population from which the small plot is drawn agrees with the map at pixel level. This is elaborated on in section 3.8.

In all cases but the two bottom rows of Tables 3-5, the indicator variable $I_{Var}$ = 0, suggesting the $SE_{CCI}$ layer provided with the biomass product is overly pessimistic about the precision of the CCI Biomass 2017 map. The considerable mean variance of plot measurement error, $mean(Var(Plt))$, of the smallest plot size category definitely contributes to this observation. Only for the highest reference biomass value $I_{Var}$ attained the value 1. Further analyses of the random error components are needed to assess whether the reported $SE_{CCI}$ for $AGB_{ref}$ > 400 Mg/ha is indeed reasonable.

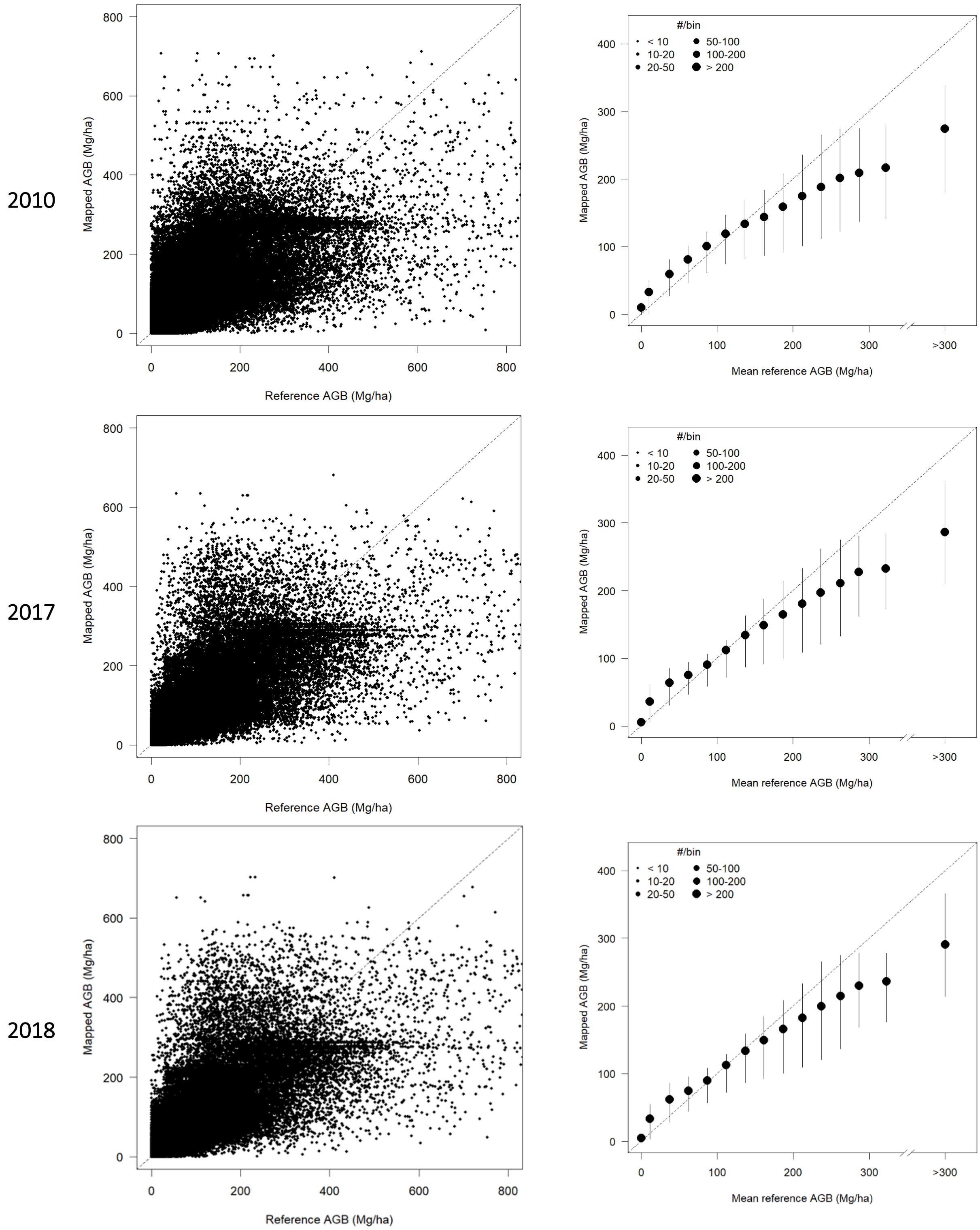


**Figure 2**. Plot-map comparisons for tier 1 data at original resolution (i.e., without spatial aggregation) for the three AGB maps; left column: scatterplots; right column: binned over 25 Mg/ha wide biomass ranges with whiskers representing the interquartile range of mapped biomass values. $AGB_{ref}$ > 350 Mg/ha data are grouped into a single bin. Note the different scales on the left and right graphs.

Table 3. Validation results per biomass range for tier 1 data at original resolution for the 2010 map.

| $AGB_{ref}$ bin | # plots | $AGB_{ref}$ | $AGB_{map}$ | $MD$ | $RMSD$ | $MSD$ | $Var(Plt)$[a] | $SE_{CCI}^2$[a] | $I_{Var}$ |
|---|---|---|---|---|---|---|---|---|---|
| [Mg/ha] | count | --------------------- | [Mg/ha] | --------------------- | | -------------- | [Mg/ha]$^2$ | ------------------ | - |
| 0-50 | 59169 | 20 | 42 | 22 | 47 | 2238 | 7816 | 566 | 0 |
| 50-100 | 28739 | 72 | 89 | 17 | 59 | 3431 | 10670 | 1836 | 0 |
| 100-150 | 13126 | 122 | 125 | 3 | 74 | 5496 | 13508 | 4744 | 0 |
| 150-200 | 6348 | 173 | 150 | -22 | 90 | 8158 | 15786 | 9254 | 0 |
| 200-250 | 3723 | 223 | 180 | -42 | 103 | 10628 | 14605 | 14600 | 0 |
| 250-300 | 2402 | 273 | 205 | -69 | 118 | 13893 | 15065 | 19458 | 0 |
| 300-400 | 2547 | 342 | 223 | -119 | 153 | 23554 | 16506 | 25954 | 0 |
| >400 | 2072 | 782 | 293 | -489 | 826 | 682269 | 48313 | 34267 | 1 |
| total | 118126 | 84 | 85 | 0 | 127 | 16098 | 10830 | 3771 | 1 |

[a] simplified notation; referring to means over biomass ranges

Table 4. Validation results per biomass range for tier 1 data at original resolution for the 2017 map.

| $AGB_{ref}$ bin | # plots | $AGB_{ref}$ | $AGB_{map}$ | $MD$ | $RMSD$ | $MSD$ | $Var(Plt)$[a] | $SE_{CCI}^2$[a] | $I_{Var}$ |
|---|---|---|---|---|---|---|---|---|---|
| [Mg/ha] | count | --------------------- | [Mg/ha] | --------------------- | | -------------- | [Mg/ha]$^2$ | ------------------ | - |
| 0-50 | 23948 | 24 | 48 | 25 | 47 | 2249 | 14698 | 884 | 0 |
| 50-100 | 18188 | 73 | 82 | 9 | 51 | 2593 | 16673 | 2046 | 0 |
| 100-150 | 11391 | 124 | 122 | -1 | 72 | 5217 | 17866 | 5274 | 0 |
| 150-200 | 5150 | 173 | 156 | -17 | 90 | 8107 | 19467 | 10568 | 0 |
| 200-250 | 3189 | 223 | 187 | -35 | 101 | 10227 | 16979 | 16060 | 0 |
| 250-300 | 2109 | 273 | 218 | -55 | 109 | 11810 | 16403 | 21482 | 0 |
| 300-400 | 2367 | 342 | 239 | -103 | 141 | 19753 | 16994 | 26680 | 0 |
| >400 | 1944 | 785 | 304 | -481 | 832 | 692944 | 48083 | 36298 | 1 |
| total | 68286 | 114 | 103 | -11 | 156 | 24215 | 17301 | 5903 | 1 |

[a] simplified notation; referring to means over biomass ranges

Table 5. Validation results per biomass range for tier 1 data at original resolution for the 2018 map.

| $AGB_{ref}$ bin [Mg/ha] | # plots count | $AGB_{ref}$ | $AGB_{map}$ | $MD$ | $RMSD$ | $MSD$ | $Var(Plt)$[a] | $SE^2_{CCI}$[a] | $I_{Var}$ |
|---|---|---|---|---|---|---|---|---|---|
| | | ---[Mg/ha]--- | | | | ---[Mg/ha]$^2$--- | | | - |
| 0-50 | 22446 | 24 | 46 | 23 | 47 | 2215 | 15656 | 771 | 0 |
| 50-100 | 17185 | 73 | 81 | 9 | 52 | 2681 | 17608 | 1743 | 0 |
| 100-150 | 10911 | 124 | 122 | -2 | 73 | 5312 | 18596 | 4767 | 0 |
| 150-200 | 4965 | 173 | 157 | -16 | 90 | 8186 | 20090 | 9431 | 0 |
| 200-250 | 3085 | 223 | 190 | -33 | 103 | 10700 | 17455 | 14951 | 0 |
| 250-300 | 2103 | 273 | 221 | -52 | 109 | 11859 | 16403 | 19673 | 0 |
| 300-400 | 2397 | 342 | 243 | -100 | 139 | 19302 | 16742 | 24816 | 0 |
| >400 | 1996 | 783 | 309 | -474 | 822 | 675817 | 47134 | 34998 | 1 |
| total | 65088 | 117 | 104 | -13 | 159 | 25312 | 18117 | 5576 | 1 |

[a] simplified notation; referring to means over biomass ranges

Table 6. Validation results per biomass range for tier 2 data at original resolution for the 2010 map.

| $AGB_{ref}$ bin [Mg/ha] | # plots count | $AGB_{ref}$ | $AGB_{map}$ | $MD$ | $RMSD$ | $MSD$ | $Var(Plt)$[a] | $SE^2_{CCI}$[a] | $I_{Var}$ |
|---|---|---|---|---|---|---|---|---|---|
| | | ---[Mg/ha]--- | | | | ---[Mg/ha]$^2$--- | | | - |
| 0-50 | 60 | 23 | 81 | 58 | 99 | 9900 | 937 | 4126 | 1 |
| 50-100 | 61 | 72 | 134 | 62 | 102 | 10414 | 216 | 3019 | 1 |
| 100-150 | 72 | 127 | 200 | 74 | 106 | 11158 | 177 | 3566 | 1 |
| 150-200 | 73 | 175 | 207 | 31 | 72 | 5179 | 602 | 4402 | 1 |
| 200-250 | 106 | 228 | 222 | -5 | 76 | 5781 | 807 | 5328 | 0 |
| 250-300 | 104 | 275 | 259 | -16 | 70 | 4866 | 239 | 6876 | 0 |
| 300-400 | 131 | 346 | 238 | -109 | 122 | 14980 | 336 | 8608 | 1 |
| >400 | 130 | 588 | 292 | -296 | 354 | 125176 | 6905 | 31095 | 1 |
| total | 737 | 274 | 220 | -54 | 172 | 29532 | 1598 | 10122 | 1 |

[a] simplified notation; referring to means over biomass ranges

## Tier 2 non-aggregated

The non-aggregated results (i.e., at original resolution) of global plot-map comparisons using tier 2 data (plot sizes 0.9 – 3 ha) are shown in Figure 3 and Tables 6-8. Spatial aggregation to 0.1° cells was omitted for this tier because of the rather limited number of available tier 2 plots.

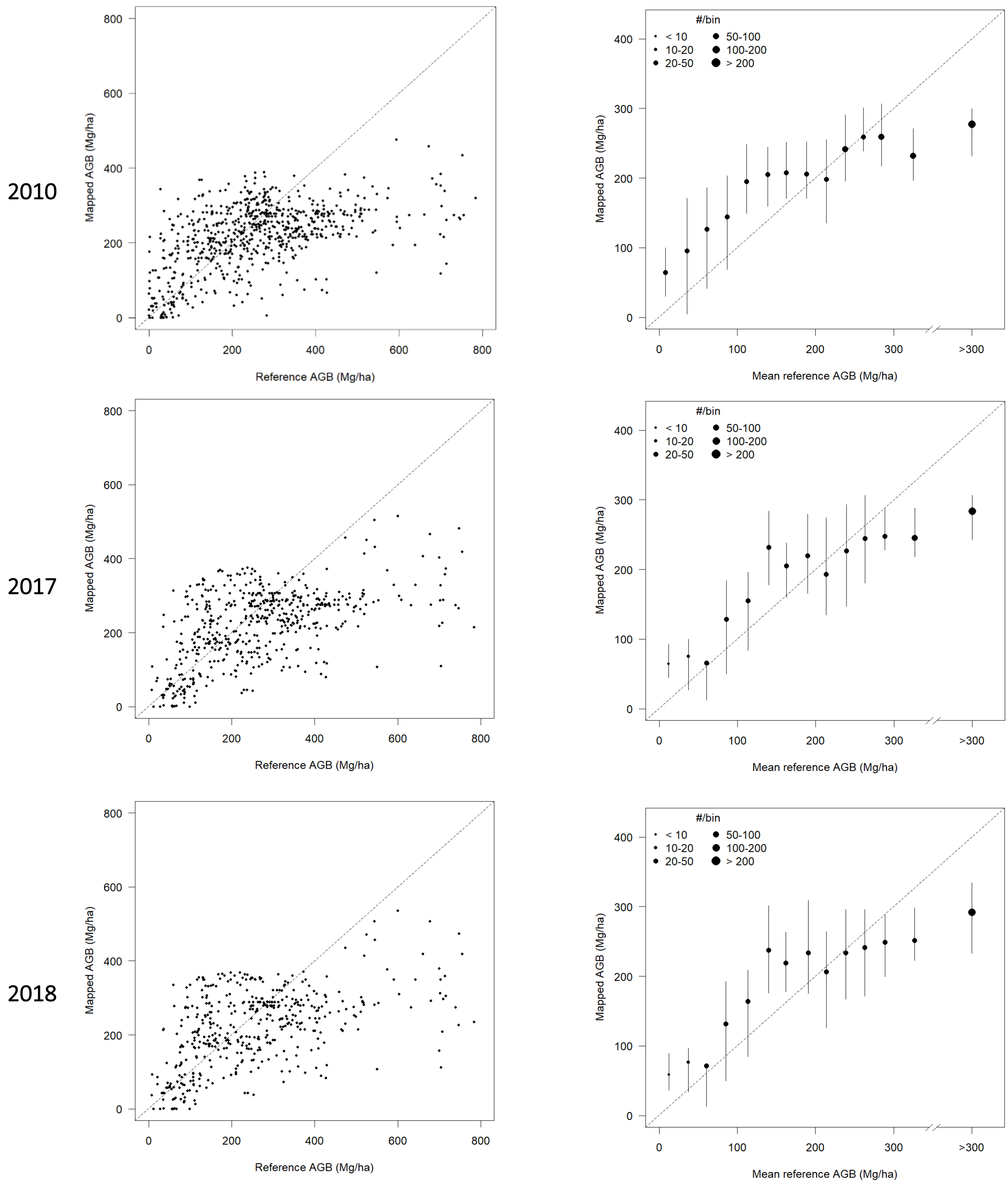


**Figure 3**. Plot-map comparisons for tier 2 data at original resolution (i.e., without spatial aggregation); left column: scatterplots; rights column: binned over 25 Mg/ha wide biomass ranges with whiskers representing the interquartile range of mapped biomass values and symbol size representing the number of plots per biomass range. $AGB_{ref}$ > 350 Mg/ha data are grouped into a single bin. Note the different scales on the left and right graphs.

Table 7. Validation results per biomass range for tier 2 data at original resolution for the 2017 map.

| $AGB_{ref}$ bin [Mg/ha] | # plots count | $AGB_{ref}$ [Mg/ha] | $AGB_{map}$ [Mg/ha] | $MD$ [Mg/ha] | $RMSD$ [Mg/ha] | $MSD$ [Mg/ha]$^2$ | $Var(Plt)$[a] [Mg/ha]$^2$ | $SE_{CCI}^2$[a] [Mg/ha]$^2$ | $I_{Var}$ - |
|---|---|---|---|---|---|---|---|---|---|
| **0-50** | 22 | 29 | 72 | 42 | 82 | 6741 | 630 | 1265 | 1 |
| **50-100** | 54 | 75 | 102 | 26 | 92 | 8419 | 162 | 2250 | 1 |
| **100-150** | 74 | 127 | 194 | 67 | 108 | 11562 | 169 | 3598 | 1 |
| **150-200** | 55 | 175 | 212 | 37 | 85 | 7226 | 200 | 4053 | 1 |
| **200-250** | 61 | 229 | 214 | -15 | 92 | 8399 | 1259 | 5349 | 1 |
| **250-300** | 78 | 275 | 246 | -29 | 79 | 6246 | 248 | 6510 | 0 |
| **300-400** | 99 | 345 | 248 | -97 | 116 | 13496 | 367 | 10729 | 1 |
| **>400** | 114 | 595 | 296 | -300 | 371 | 137733 | 7425 | 31481 | 1 |
| **total** | 557 | 289 | 222 | -68 | 189 | 35715 | 1840 | 10994 | 1 |

[a] simplified notation; referring to means over biomass ranges

Table 8. Validation results per biomass range for tier 2 data at original resolution for the 2018 map.

| $AGB_{ref}$ bin [Mg/ha] | # plots count | $AGB_{ref}$ [Mg/ha] | $AGB_{map}$ [Mg/ha] | $MD$ [Mg/ha] | $RMSD$ [Mg/ha] | $MSD$ [Mg/ha]$^2$ | $Var(Plt)$[a] [Mg/ha]$^2$ | $SE_{CCI}^2$[a] [Mg/ha]$^2$ | $I_{Var}$ - |
|---|---|---|---|---|---|---|---|---|---|
| **0-50** | 22 | 30 | 71 | 41 | 76 | 5833 | 630 | 1245 | 1 |
| **50-100** | 55 | 75 | 107 | 31 | 97 | 9486 | 178 | 2256 | 1 |
| **100-150** | 74 | 127 | 202 | 74 | 115 | 13245 | 169 | 3881 | 1 |
| **150-200** | 47 | 176 | 226 | 50 | 94 | 8926 | 188 | 4458 | 1 |
| **200-250** | 52 | 229 | 223 | -6 | 91 | 8278 | 1443 | 5494 | 1 |
| **250-300** | 63 | 275 | 245 | -30 | 78 | 6119 | 259 | 6548 | 0 |
| **300-400** | 83 | 346 | 254 | -92 | 116 | 13402 | 395 | 9875 | 1 |
| **>400** | 89 | 635 | 306 | -330 | 403 | 162300 | 9401 | 40546 | 1 |
| **total** | 485 | 282 | 223 | -59 | 195 | 37985 | 2074 | 11906 | 1 |

[a] simplified notation; referring to means over biomass ranges

In general, over-prediction of biomass is observed for reference biomass values up to 200 Mg/ha, while above 250 Mg/ha biomass is under-predicted by the CCI Biomass maps. The under-prediction increases with reference biomass and reaches maxima of 296 Mg/ha (2010), 300 Mg/ha (2017) and 330 Mg/ha (2018) for mean reference biomass densities of 588, 595 and 635 Mg/ha, respectively.

In most cases, the indicator variable $I_{Var}$ = 1. In contrast to the small plots in tier 1, the $mean(Var(Plt))$ estimates of larger plots in tier 2 are much lower, which contributes to this result. It does not necessarily imply that the $SE_{CCI}$ layer provided with the biomass product is too *optimistic* about the precision of the CCI Biomass maps since positional error and within-pixel sampling error may also contribute to observed differences between $AGB_{map}$ and $AGB_{ref}$ (see PVPs). However, note that the within-pixel sampling error will be small since the plots in this tier are comparable in size or even larger than the map pixels. The effect of positional error plays a role in areas with AGB gradients and needs further analysis.

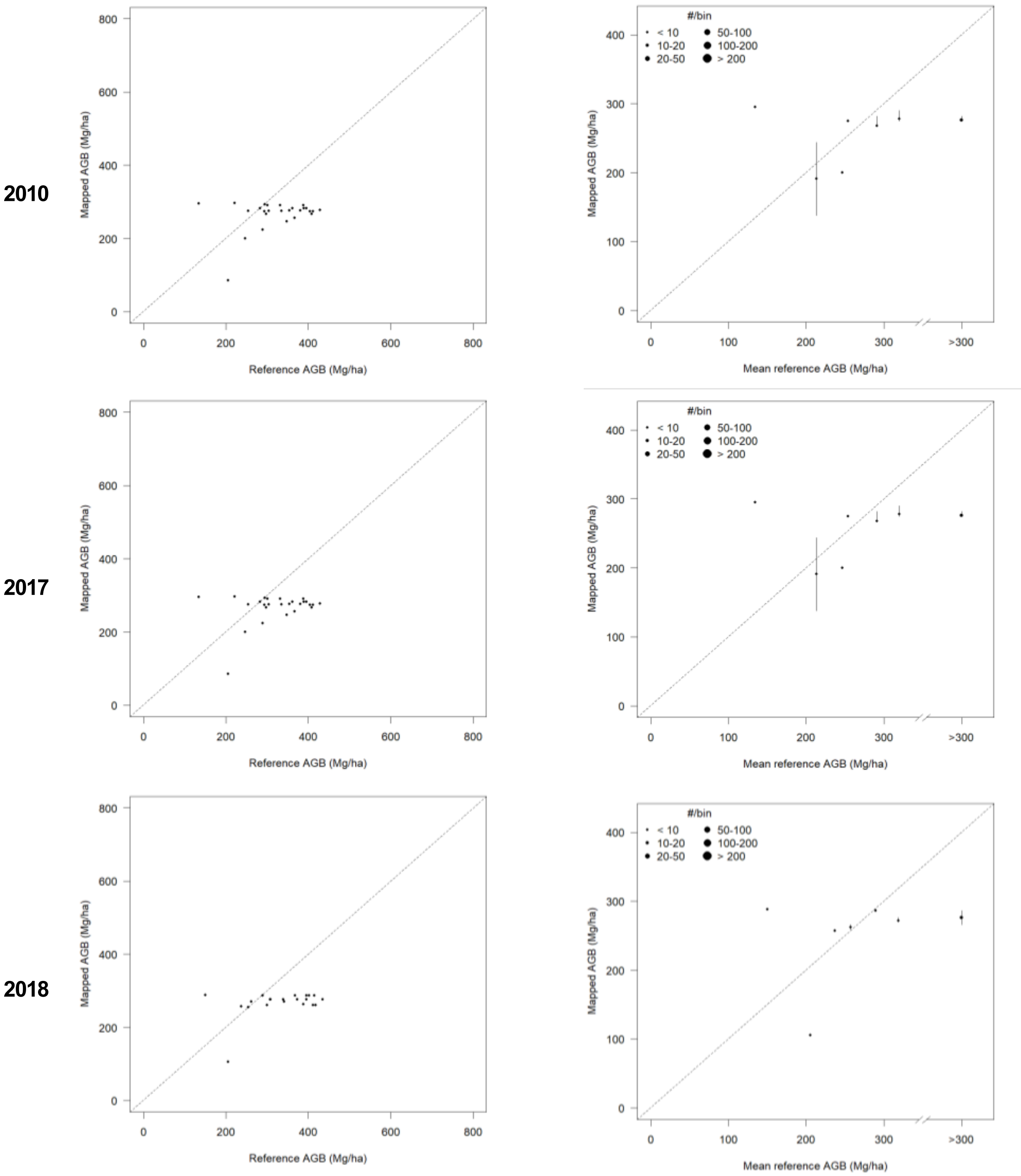


**Figure 4**. Plot-map comparisons for tier 3 data at original resolution (i.e., without spatial aggregation); left column: scatterplots; right column: binned over 25 Mg/ha wide biomass ranges with whiskers representing the interquartile range of mapped biomass values and symbol size representing the number of plots per biomass range. $AGB_{ref}$ > 350 Mg/ha data are grouped into a single bin. Note the different scales in the left and right graphs.

## Tier 3 non-aggregated

The non-aggregated results (i.e., at original plot level) of global plot-map comparisons using tier 3 data (plot size ≥ 6 ha) are shown in Figure 4 and Tables 9-11. Similar to tier 2, spatial aggregation to 0.1° cells was omitted because of the small number of available tier 3 plots.

It is important to note that most tier 3 plots are in the tropics and cover a biomass range between 150 and 450 Mg/ha (i.e., the biomass range where SAR sensors lose sensitivity), so lack low biomass densities. The small number of plots and the large scatter hardly allow conclusions to be drawn based on these data, except for the general trend of the map to under-predict biomass in the higher part of the assessed biomass range, which was also observed with the tier 1-2 data.

Table 9. Validation results per biomass range for tier 3 data at the original resolution for the 2010 map.

| $AGB_{ref}$ bin | # plots | $AGB_{ref}$ | $AGB_{map}$ | $MD$ | $RMSD$ | $MSD$ | $Var(Plt)$[a] | $SE^2_{CCI}$[a] | $I_{Var}$ |
|---|---|---|---|---|---|---|---|---|---|
| [Mg/ha] | count | ---------------------[Mg/ha] | | | --------------------- | --------------[Mg/ha]$^2$ | | ----------------- - | - |
| 0-50 | - | - | - | - | - | - | - | - | - |
| 50-100 | - | - | - | - | - | - | - | - | - |
| 100-150 | 1 | 134 | 295 | 161 | 161 | 25893 | 70 | 9216 | 1 |
| 150-200 | - | - | - | - | - | - | - | - | - |
| 200-250 | 3 | 225 | 194 | -30 | 86 | 7436 | 459 | 6719 | 1 |
| 250-300 | 6 | 285 | 269 | -16 | 31 | 991 | 167 | 5978 | 0 |
| 300-400 | 13 | 350 | 278 | -72 | 81 | 6581 | 176 | 7165 | 0 |
| >400 | 4 | 413 | 273 | -139 | 139 | 19435 | 214 | 6680 | 1 |
| total | 27 | 323 | 267 | -56 | 90 | 8053 | 207 | 6856 | 1 |

[a] simplified notation; referring to means over the biomass ranges

Table 10. Validation results per biomass range for tier 3 data at the original resolution for the 2017 map.

| $AGB_{ref}$ bin [Mg/ha] | # plots count | $AGB_{ref}$ | $AGB_{map}$ | $MD$ | $RMSD$ | $MSD$ | $Var(Plt)$[a] | $SE^2_{CCI}$[a] | $I_{Var}$ |
|---|---|---|---|---|---|---|---|---|---|
| | | [Mg/ha] | | | | [Mg/ha]$^2$ | | | - |
| 0-50 | - | - | - | - | - | - | - | - | - |
| 50-100 | - | - | - | - | - | - | - | - | - |
| 100-150 | - | - | - | - | - | - | - | - | - |
| 150-200 | 1 | 150 | 293 | 142 | 142 | 20246 | 70 | 8464 | 1 |
| 200-250 | 2 | 220 | 191 | -30 | 73 | 5376 | 611 | 3946 | 1 |
| 250-300 | 3 | 268 | 274 | 6 | 14 | 200 | 151 | 7360 | 0 |
| 300-400 | 12 | 344 | 290 | -54 | 66 | 4375 | 169 | 5963 | 0 |
| >400 | 5 | 416 | 284 | -132 | 133 | 17803 | 208 | 7198 | 1 |
| total | 23 | 331 | 278 | -53 | 87 | 7527 | 209 | 6347 | 1 |

[a] simplified notation; referring to means over the biomass ranges

Table 11. Validation results per biomass range for tier 3 data at the original resolution for the 2018 map.

| $AGB_{ref}$ bin [Mg/ha] | # plots count | $AGB_{ref}$ | $AGB_{map}$ | $MD$ | $RMSD$ | $MSD$ | $Var(Plt)$[a] | $SE^2_{CCI}$[a] | $I_{Var}$ |
|---|---|---|---|---|---|---|---|---|---|
| | | [Mg/ha] | | | | [Mg/ha]$^2$ | | | - |
| 0-50 | - | - | - | - | - | - | - | - | - |
| 50-100 | - | - | - | - | - | - | - | - | - |
| 100-150 | - | - | - | - | - | - | - | - | - |
| 150-200 | 1 | 150 | 288 | 138 | 138 | 19055 | 70 | 9216 | 1 |
| 200-250 | 2 | 221 | 181 | -40 | 72 | 5213 | 611 | 5661 | 0 |
| 250-300 | 3 | 268 | 271 | 2 | 6 | 31 | 151 | 8034 | 0 |
| 300-400 | 10 | 351 | 275 | -77 | 84 | 7026 | 169 | 7325 | 0 |
| >400 | 5 | 416 | 274 | -142 | 143 | 20395 | 208 | 7149 | 1 |
| total | 21 | 333 | 266 | -67 | 98 | 9610 | 213 | 7316 | 1 |

[a] simplified notation; referring to means over the biomass ranges

## 3.2. Tier 1 plot data spatially aggregated to 0.1° cells

The results of global $AGM_{map}$ - $AGB_{ref}$ comparisons using tier 1 data (plot size ≤ 0.6 ha) spatially aggregated to 0.1° cells are shown in Figure 5 and Tables 12-14. The rightmost variance columns shown in Tables 3-11 are omitted here because spatial correlation of errors within 0.1° cells may be non-negligible but we lack data to assess such correlation for most biomes at the current stage of the project.

Spatial aggregation to 0.1° cells improved the fit between $AGB_{ref}$ and $AGB_{map}$. The higher reference biomass is still under-predicted, but up to 300 Mg/ha, except for peaks around $AGB_{ref} \approx 200$ Mg/ha, the absolute mean differences are within 30 Mg/ha. The 0.1° cells producing the peak at $AGB_{ref} \approx 200$ Mg/ha are located in east Australia (not shown here).

Apart from the above issue, spatial aggregation successfully reduced the effect of localized AGB fluctuations in the map and their potential interaction with plot-map geolocation mismatches. These results (Figure 5, Tables 12-14) suggest the CCI Biomass predictions at 0.1° cell resolution are more accurate than at the original pixel resolution. As we will see later, very similar results were obtained for the temperate broadleaf and mixed forest biome. Most 0.1° cells meeting the criterion of at least five plots per cell happen to be located in that biome.

Table 12. Validation results per biomass range for tier 1 data spatially aggregated to 0.1° cells for the 2010 map.

| $AGB_{ref}$ bin [Mg/ha] | # cells count | $AGB_{ref}$ | $AGB_{map}$ | $MD$ | $RMSD$ |
|---|---|---|---|---|---|
| | | ---[Mg/ha]--- | | | |
| 0-50 | 3809 | 23 | 33 | 10 | 26 |
| 50-100 | 1847 | 70 | 80 | 10 | 34 |
| 100-150 | 506 | 121 | 136 | 16 | 83 |
| 150-200 | 194 | 171 | 195 | 24 | 94 |
| 200-250 | 127 | 226 | 223 | -3 | 84 |
| 250-300 | 90 | 273 | 249 | -24 | 81 |
| 300-400 | 49 | 338 | 261 | -77 | 110 |
| >400 | 48 | 700 | 365 | -335 | 430 |
| total | 6670 | 62 | 69 | 7 | 56 |

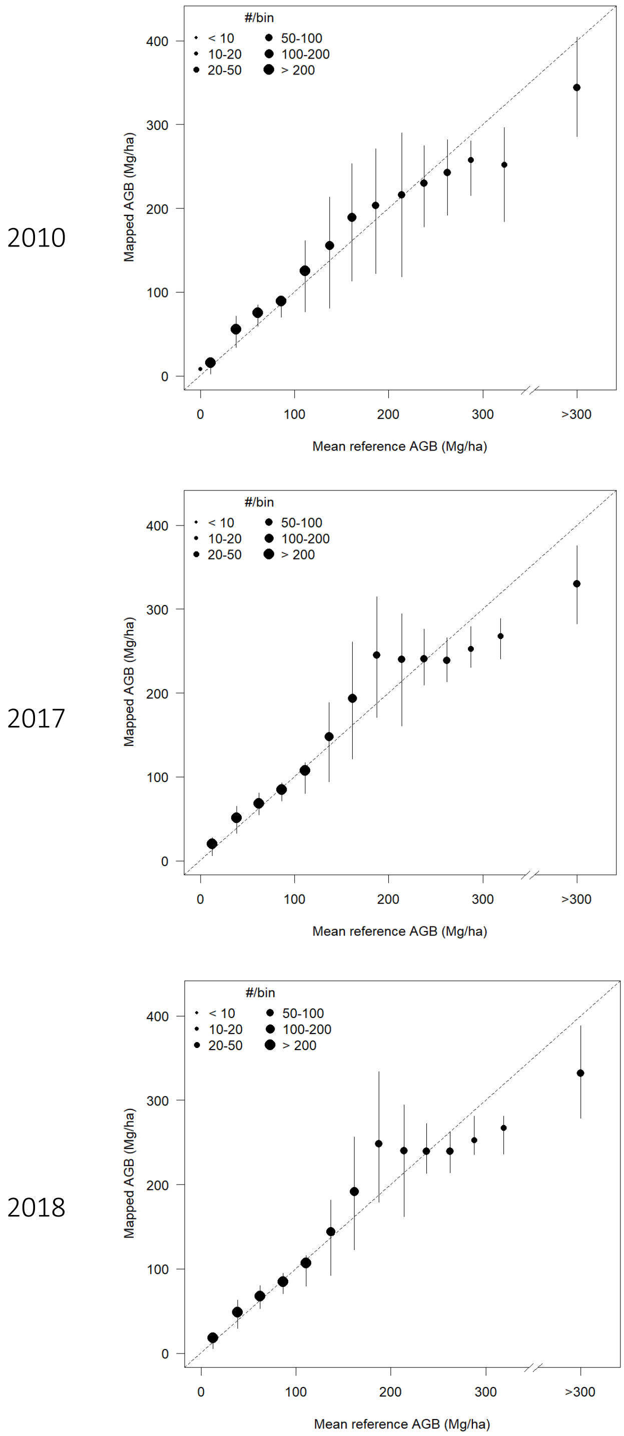


**Figure 5**. AGBref - AGMmap comparisons for tier 1 data spatially aggregated to 0.1° and binned over 25 Mg/ha wide biomass ranges with whiskers representing the interquartile range of mapped biomass values and symbol size representing the number of 0.1° cells per biomass range. AGBref > 350 Mg/ha data are grouped into a single bin.

Table 13. Validation results per biomass range for tier 1 data spatially aggregated to 0.1° cells for the 2017 map.

| $AGB_{ref}$ bin | # cells | $AGB_{ref}$ | $AGB_{map}$ | *MD* | *RMSD* |
|---|---|---|---|---|---|
| [Mg/ha] | count | ---------------------[Mg/ha] --------------------- | | | |
| 0-50 | 1664 | 27 | 37 | 10 | 24 |
| 50-100 | 1646 | 72 | 75 | 3 | 27 |
| 100-150 | 554 | 120 | 122 | 2 | 59 |
| 150-200 | 173 | 172 | 215 | 43 | 102 |
| 200-250 | 113 | 225 | 240 | 15 | 89 |
| 250-300 | 93 | 273 | 245 | -28 | 64 |
| 300-400 | 54 | 337 | 274 | -62 | 103 |
| >400 | 52 | 690 | 346 | -344 | 437 |
| total | 4349 | 84 | 86 | 2 | 64 |

Table 14. Validation results per biomass range for tier 1 data spatially aggregated to 0.1° cells for the 2018 map.

| $AGB_{ref}$ bin | # cells | $AGB_{ref}$ | $AGB_{map}$ | *MD* | *RMSD* |
|---|---|---|---|---|---|
| [Mg/ha] | count | ---------------------[Mg/ha] --------------------- | | | |
| 0-50 | 1659 | 27 | 35 | 8 | 23 |
| 50-100 | 1649 | 72 | 75 | 3 | 27 |
| 100-150 | 553 | 120 | 120 | 0 | 60 |
| 150-200 | 173 | 172 | 215 | 43 | 108 |
| 200-250 | 113 | 225 | 240 | 15 | 96 |
| 250-300 | 93 | 272 | 245 | -28 | 68 |
| 300-400 | 54 | 337 | 276 | -60 | 107 |
| >400 | 52 | 690 | 346 | -344 | 437 |
| total | 4346 | 84 | 85 | 1 | 65 |

## 3.3. Comparisons with LiDAR-based and 1-km pixel Congo basin Forests AGB

The results of the global $AGM_{map}$ - $AGB_{re}$ comparisons at 0.1° resolution using LiDAR-based and CoFor AGB as reference data are shown in Figure 6 and Tables 15-17.

.

The key observation, common to all three AGB maps, is the map underestimation starting at 300 Mg/ha. This effect may be influenced by the CoFor data having a dense plot network in the forest management areas of Congo basin. Since the original plot data inside the 1-km aggregates of the CoFor dataset are unavailable, we were unable to account for partly deforested areas. Such areas are likely to exist given the active forestry activities in the area. On the other hand, similar results were observed using the plot data, which builds confidence in using LiDAR and CoFor data for accuracy assessments.

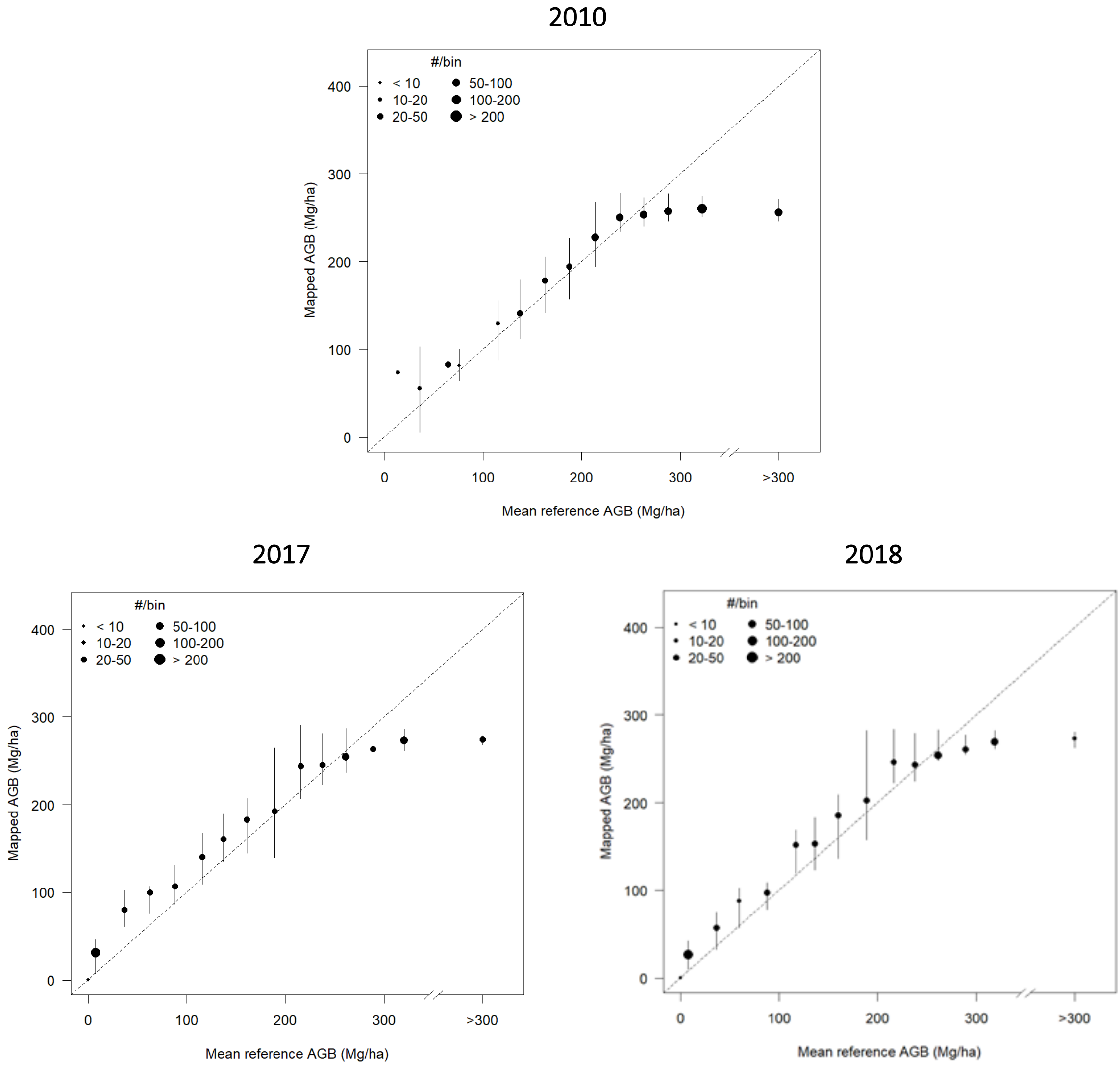


**Figure 6.** AGBref - AGMmap comparisons for LiDAR-based and CoFor AGB data spatially aggregated to 0.1° and binned over 25 Mg/ha wide biomass ranges with whiskers representing the interquartile range of mapped biomass values and symbol size representing the number of 0.1° cells per biomass range. AGBref > 350 Mg/ha data are grouped into a single bin.

Table 15. Validation results per biomass range using LiDAR-based and CoFor AGB data spatially aggregated to 0.1° cells for the 2010 map.

| $AGB_{ref}$ bin [Mg/ha] | # cells count | $AGB_{ref}$ | $AGB_{map}$ | $MD$ | $RMSD$ |
|---|---|---|---|---|---|
| | | ----------[Mg/ha]---------- | | | |
| 0-50 | 30 | 27 | 63 | 36 | 65 |
| 50-100 | 24 | 66 | 83 | 16 | 51 |
| 100-150 | 37 | 130 | 137 | 7 | 45 |
| 150-200 | 51 | 175 | 187 | 11 | 55 |
| 200-250 | 117 | 227 | 240 | 12 | 51 |
| 250-300 | 174 | 276 | 256 | -20 | 42 |
| 300-400 | 204 | 333 | 259 | -74 | 84 |
| >400 | 25 | 450 | 259 | -191 | 204 |
| total | 662 | 257 | 227 | -30 | 73 |

Table 16. Validation results per biomass range using LiDAR-based and CoFor AGB data spatially aggregated to 0.1° cells for the 2017 map.

| $AGB_{ref}$ bin [Mg/ha] | # cells count | $AGB_{ref}$ | $AGB_{map}$ | $MD$ | $RMSD$ |
|---|---|---|---|---|---|
| | | ----------[Mg/ha]---------- | | | |
| 0-50 | 141 | 14 | 42 | 28 | 44 |
| 50-100 | 62 | 77 | 104 | 27 | 47 |
| 100-150 | 63 | 128 | 151 | 24 | 45 |
| 150-200 | 62 | 172 | 187 | 15 | 58 |
| 200-250 | 81 | 226 | 244 | 18 | 55 |
| 250-300 | 93 | 274 | 259 | -15 | 44 |
| 300-400 | 72 | 331 | 274 | -57 | 65 |
| >400 | 5 | 438 | 270 | -167 | 169 |
| total | 579 | 164 | 170 | 5 | 53 |

Table 17. Validation results per biomass range using LiDAR-based and CoFor AGB data spatially aggregated to 0.1° cells for the 2018 map

| $AGB_{ref}$ bin [Mg/ha] | # cells count | $AGB_{ref}$ | $AGB_{map}$ | *MD* | *RMSD* |
|---|---|---|---|---|---|
| | | ---------------------[Mg/ha] | --------------------- | | |
| 0-50 | 128 | 13 | 32 | 19 | 29 |
| 50-100 | 41 | 77 | 94 | 17 | 41 |
| 100-150 | 45 | 126 | 153 | 27 | 51 |
| 150-200 | 53 | 171 | 192 | 21 | 65 |
| 200-250 | 76 | 225 | 245 | 20 | 55 |
| 250-300 | 93 | 274 | 257 | -17 | 44 |
| 300-400 | 58 | 326 | 270 | -56 | 62 |
| >400 | 3 | 446 | 265 | -181 | 183 |
| total | 497 | 166 | 169 | 3 | 50 |

## 3.4.Summary tables on tier 1-3 comparisons

To facilitate interpretation, the bias and RMSD estimates per map for different $AGB_{ref}$ bins differentiated by tier are shown in Table 21 and Table 19, respectively. Figure 7 provides the legend for the colour schemes used in these tables.

Table 21 shows that for the mid-range of $AGB_{ref}$, bias tends to be within 20% of $AGB_{ref}$. The 100-150 bin of tier 2 and the 150-200 Mg/ha bin of tier 3 are exceptions. AGB between 250 and 400 Mg/ha appears to be within 30% of $AGB_{ref.}$ However, these are each based on data from a single plot. At the lower and upper ends of the considered AGB range, bias mostly exceeds the 20% threshold. The RMSD exceeds the 20% threshold in all cases but the 250-300 Mg/ha bin for tier 2 and extending until the 300-400 Mg/ha bin for tier 3 (Table 19).

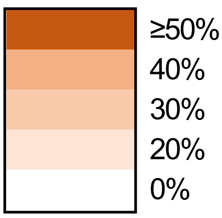


**Figure 7**. Legend for colour schemes used in summary tables of bias and RMSD.

Table 18. AGB bias [Mg/ha] differentiated per tier and per AGB bin. Colour shading is based on relative bias; legend in Figure 7.

| | Original resolution | | | | | | | | | 0.1° cells tier 1 | | |
|---|---|---|---|---|---|---|---|---|---|---|---|---|
| AGB bin | Tier 1 | | | Tier 2 | | | Tier 3 | | | | | |
| | 2010 | 2017 | 2018 | 2010 | 2017 | 2018 | 2010 | 2017 | 2018 | 2010 | 2017 | 2018 |
| 0-50 | 22 | 25 | 23 | 58 | 42 | 41 | - | - | - | 10 | 10 | 8 |
| 50-100 | 17 | 9 | 9 | 62 | 26 | 31 | - | - | - | 10 | 3 | 3 |
| 100-150 | 3 | -1 | -2 | 74 | 67 | 74 | 161 | - | - | 16 | 2 | 0 |
| 150-200 | -22 | -17 | -16 | 31 | 37 | 50 | - | 142 | 138 | 24 | 43 | 43 |
| 200-250 | -42 | -35 | -33 | -5 | -15 | -6 | -30 | -30 | -40 | -3 | 15 | 15 |
| 250-300 | -69 | -55 | -52 | -16 | -29 | -30 | -16 | 6 | 2 | -24 | -28 | -28 |
| 300-400 | -119 | -103 | -100 | -109 | -97 | -92 | -72 | -54 | -77 | -77 | -62 | -60 |
| >400 | -489 | -481 | -474 | -296 | -300 | -330 | -139 | -132 | -142 | -335 | -344 | -344 |

Table 19. Root mean square difference (RMSD) differentiated per tier and per AGB bin.

| | Original resolution | | | | | | | | | 0.1° cells tier 1 | | |
|---|---|---|---|---|---|---|---|---|---|---|---|---|
| | Tier 1 | | | Tier 2 | | | Tier 3 | | | | | |
| | 2010 | 2017 | 2018 | 2010 | 2017 | 2018 | 2010 | 2017 | 2018 | 2010 | 2017 | 2018 |
| 0-50 | 47 | 47 | 47 | 99 | 82 | 76 | - | - | - | 26 | 24 | 23 |
| 50-100 | 59 | 51 | 52 | 102 | 92 | 97 | | - | - | 34 | 27 | 27 |
| 100-150 | 74 | 72 | 73 | 106 | 108 | 115 | 161 | - | - | 83 | 59 | 60 |
| 150-200 | 90 | 90 | 90 | 72 | 85 | 94 | - | 142 | 138 | 94 | 102 | 108 |
| 200-250 | 103 | 101 | 103 | 76 | 92 | 91 | 86 | 73 | 72 | 84 | 89 | 96 |
| 250-300 | 118 | 109 | 109 | 70 | 79 | 78 | 31 | 14 | 6 | 81 | 64 | 68 |
| 300-400 | 153 | 141 | 139 | 122 | 116 | 116 | 81 | 66 | 84 | 110 | 103 | 107 |
| >400 | 826 | 832 | 822 | 354 | 371 | 403 | 139 | 133 | 143 | 430 | 437 | 437 |

## 3.5. Assessments by ecoregion

To allow assessments of validation results over different ecoregions, spatially aggregated comparisons of $AGB_{ref}$ and $AGM_{map}$ were stratified by biomes (Dinerstein et al., 2017). Results are presented in Figures 8-10 and in Appendix B. Several strata had limited data or no data at all (e.g., deserts, flooded grassland, etc.). These cases are not included here.

For the boreal forests, mangroves, temperate grasslands, savannahs and shrublands, and tropical and subtropical grasslands, savannahs and shrublands biomes, reasonable fits with minor over-predictions are found in the lower AGB ranges. Map over-prediction is least observed in temperate broadleaf and mixed forests, while map under-prediction is most present in tropical and subtropical dry broadleaf forest. Note that data in the dry tropical regions are limited, which hampers drawing solid conclusions. Spikes of map over-prediction were also found in the Mediterranean forests, woodland and scrub around the 200Mg/ha bin, particularly in the 2017 and 2018 maps. The $AGB_{ref}$ density at which under-prediction starts differs per biome. For the boreal forests and tundra, saturation of $AGB_{map}$ occurs at approximately 100 Mg/ha, for example. The strong similarity of results for the temperate broadleaf and mixed forests biome (Figures 8-10) with those of the spatially aggregated results obtained with the tier 1 data (Figure 5) was already mentioned above.

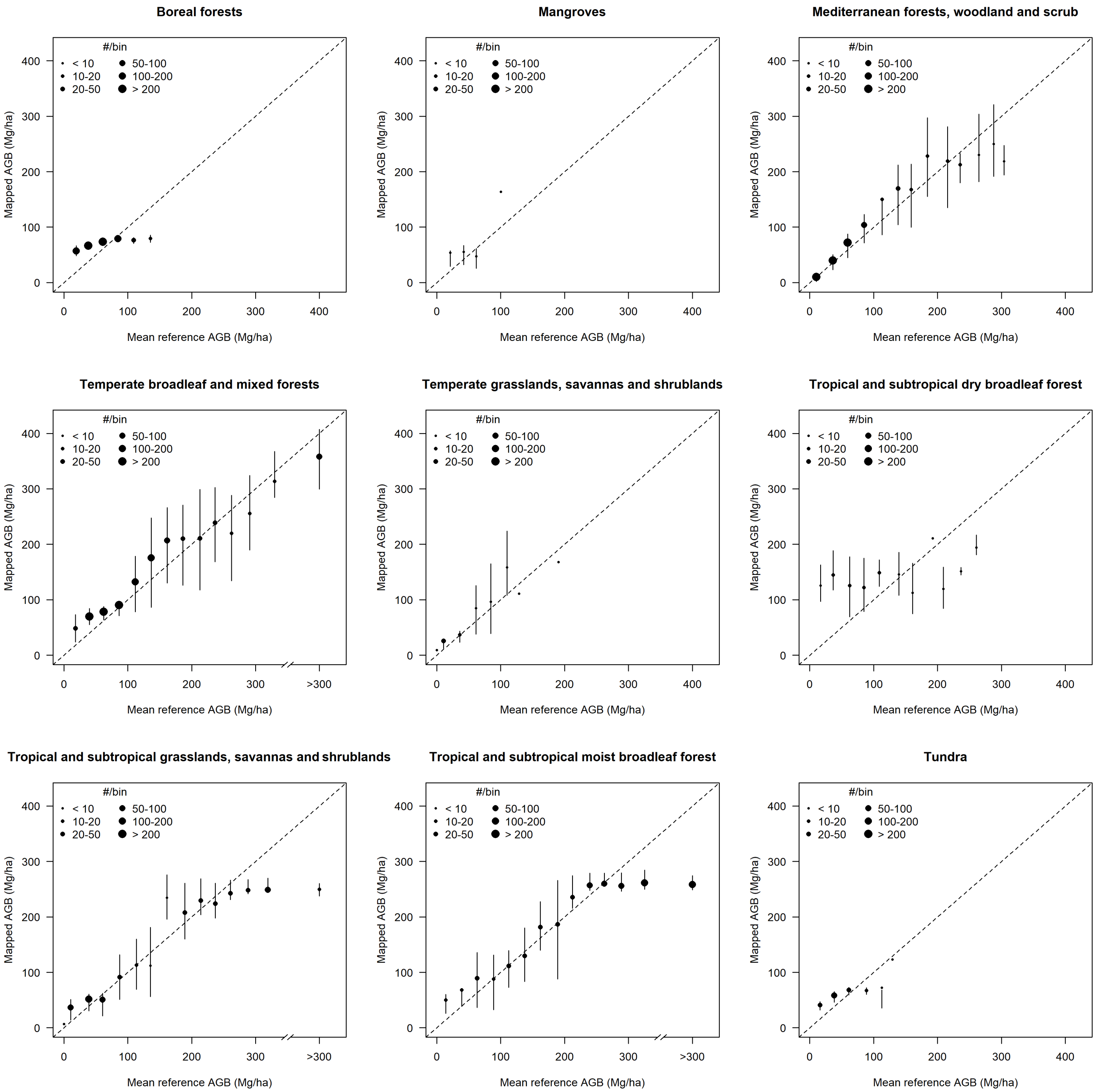


**Figure 8**. Comparisons between $AGB_{ref}$ and the **2010** AGB map per biome (Dinerstein et al., 2017) using all available data binned over 25 Mg/ha wide biomass ranges with whiskers representing the interquartile range of mapped biomass values and symbol size representing the number of 0.1° cells per biomass range.

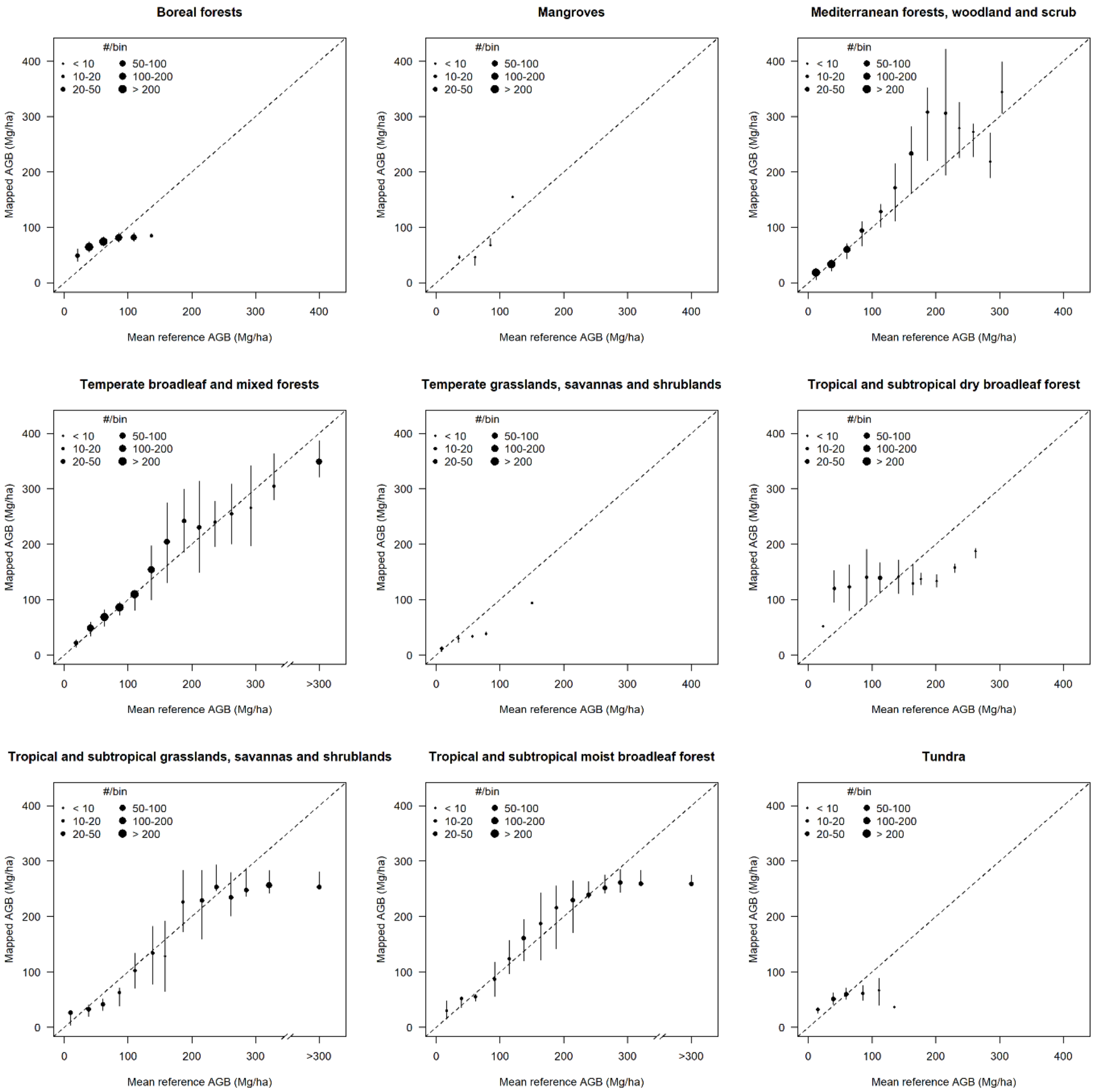


**Figure 9**. Comparisons between $AGB_{ref}$ and the **2017** AGB map per biome (Dinerstein et al., 2017) using all available data binned over 25 Mg/ha wide biomass ranges with whiskers representing the interquartile range of mapped biomass values and symbol size representing the number of 0.1° cells per biomass range.

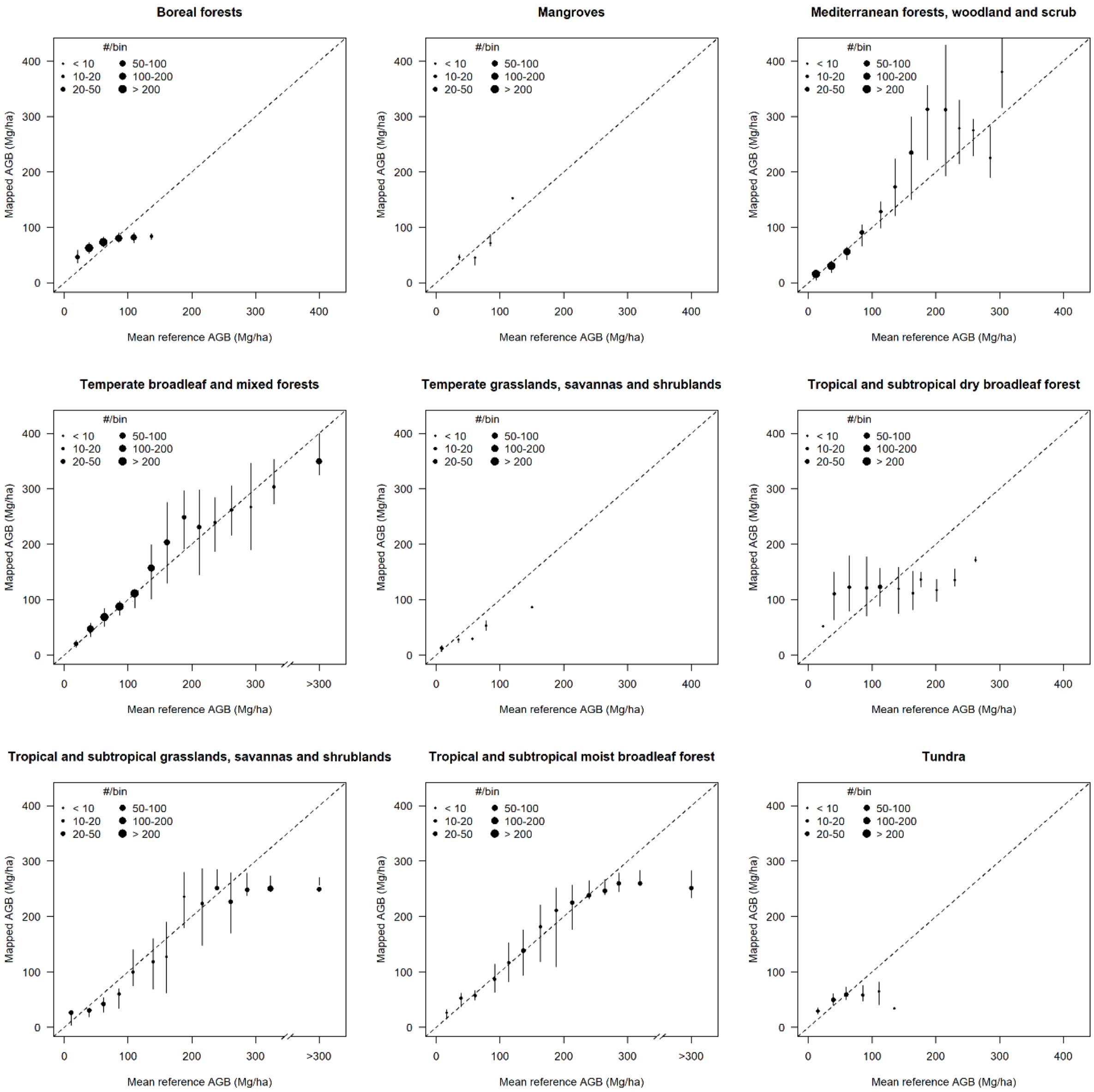


**Figure 10**. Comparisons between $AGB_{ref}$ and the **2018** AGB map per biome (Dinerstein et al., 2017) using all available data binned over 25 Mg/ha wide biomass ranges with whiskers representing the interquartile range of mapped biomass values and symbol size representing the number of 0.1° cells per biomass range.

## 3.6. Summary tables of the assessments by ecoregion

To facilitate interpretation per AGB map, the bias and RMSD estimates for different $AGB_{ref}$ bins differentiated by biome are shown from Table 20 to Table 25.

The tables re-emphasize our overall finding that in the lower and higher biomass ranges the bias and RMSD are larger than for the mid-ranges. The bias for the mid-ranges for most biomes is around or below 20%, while the RMSD is above 20%.

The quantity of available reference information varies for different regions and there is lower confidence for some with limited reference data, including the (sub-)tropical dry forests and grasslands, mangroves, temperate grasslands and tundra.

Table 20. AGB bias [Mg/ha] differentiated per biome and per AGB bin for the 2010 map. Colour shading is based the legend shown in Figure 7.

| $AGB_{ref}$ [Mg/ha] | Boreal | Mangrove | Mediterranean | Temperate broadleaf/mixed | Temperate grasslands, savannas and shrublands | Tropical/subtropical dry broadleaf | tropical and subtropical grasslands | Tropical and subtropical moist broadleaf forest | Tundra |
|---|---|---|---|---|---|---|---|---|---|
| 0-50 | 30 | 21 | 1 | 30 | 10 | 108 | 17 | 32 | 21 |
| 50-100 | 7 | -14 | 14 | 11 | 17 | 50 | -5 | 14 | -3 |
| 100-150 | -38 | 64 | 34 | 27 | 41 | 27 | -11 | -4 | -35 |
| 150-200 | - | - | 26 | 37 | -23 | -41 | 33 | 9 | - |
| 200-250 | - | - | -7 | 0 | - | -88 | 1 | 20 | - |
| 250-300 | - | - | -36 | -39 | - | -67 | -28 | -18 | - |
| 300-400 | - | - | -85 | -33 | - | - | -76 | -84 | - |
| >400 | - | - | - | -333 | - | - | -209 | -171 | - |
| Total | 16 | 9 | 3 | 9 | 15 | 41 | -8 | -38 | 11 |

Table 21. Root mean square difference (RMSD) differentiated per biome and per AGB bin for the 2010 map. Colour shading is based the legend shown in Figure 7; column headings are as above.

| | | | | | | | | | |
|---|---|---|---|---|---|---|---|---|---|
| 0-50 | 32 | 47 | 15 | 37 | 25 | 120 | 41 | 61 | 28 |
| 50-100 | 16 | 26 | 37 | 35 | 55 | 73 | 43 | 61 | 25 |
| 100-150 | 40 | 64 | 101 | 90 | 89 | 61 | 58 | 59 | 59 |
| 150-200 | - | - | 94 | 100 | 23 | 67 | 73 | 77 | - |
| 200-250 | - | - | 87 | 99 | - | 93 | 59 | 54 | - |
| 250-300 | - | - | 91 | 102 | - | 73 | 50 | 46 | - |
| 300-400 | - | - | 96 | 96 | - | - | 89 | 95 | - |
| >400 | - | - | - | 429 | - | - | 213 | 176 | - |
| Total | 27 | 41 | 26 | 92 | 45 | 86 | 58 | 82 | 29 |

Table 22. AGB bias [Mg/ha] differentiated per biome and per AGB bin for the 2017 map. Colour shading is based the legend shown in Figure 7.

| $AGB_{ref}$ [Mg/ha] | Boreal | Mangrove | Mediterranean | Temperate broadleaf/mixed | Temperate grasslands, savannas and shrublands | Tropical/subtropical dry broadleaf | tropical and subtropical grasslands | Tropical and subtropical moist broadleaf forest | Tundra |
|---|---|---|---|---|---|---|---|---|---|
| 0-50 | 26 | 10 | 3 | 7 | 3 | 76 | 4 | 13 | 13 |
| 50-100 | 7 | -16 | 1 | 2 | -31 | 53 | -20 | -5 | -7 |
| 100-150 | -33 | 35 | 26 | 5 | -56 | 21 | -7 | 19 | -55 |
| 150-200 | - | - | 90 | 48 | - | -36 | 20 | 26 | - |
| 200-250 | - | - | 76 | 12 | - | -70 | 14 | 7 | - |
| 250-300 | - | - | -21 | -13 | - | -75 | -33 | -19 | - |
| 300-400 | - | - | - | -21 | - | - | -77 | -82 | - |
| >400 | - | - | - | -341 | - | - | -214 | -197 | - |
| Total | 12 | -7 | 7 | -6 | -6 | 23 | -25 | -22 | -1 |

Table 23. Root mean square difference (RMSD) differentiated per biome and per AGB bin for the 2017 map. Colour shading is based the legend shown in Figure 7; column headings are as above.

| | | | | | | | | | |
|---|---|---|---|---|---|---|---|---|---|
| 0-50 | 29 | 12 | 19 | 20 | 8 | 84 | 36 | 29 | 19 |
| 50-100 | 17 | 31 | 27 | 29 | 33 | 76 | 32 | 29 | 20 |
| 100-150 | 37 | 35 | 69 | 63 | 56 | 42 | 48 | 54 | 66 |
| 150-200 | - | - | 137 | 99 | - | 53 | 72 | 85 | - |
| 200-250 | - | - | 133 | 93 | - | 72 | 67 | 61 | - |
| 250-300 | - | - | 84 | 77 | - | 78 | 64 | 44 | - |
| 300-400 | - | - | - | 77 | - | - | 91 | 94 | - |
| >400 | - | - | - | 436 | - | - | 226 | 210 | - |
| Total | 24 | 29 | 38 | 95 | 20 | 65 | 66 | 75 | 27 |

Table 24. AGB bias [Mg/ha] differentiated per biome and per AGB bin for the 2018 map. Colour shading is based the legend shown in Figure 7.

| $AGB_{ref}$ [Mg/ha] | Boreal | Mangrove | Mediterranean | Temperate broadleaf/mixed | Temperate grasslands, savannas and shrublands | Tropical/subtropical dry broadleaf | tropical and subtropical grasslands | Tropical and subtropical moist broadleaf forest | Tundra |
|---|---|---|---|---|---|---|---|---|---|
| 0-50 | 24 | 10 | 0 | 5 | 2 | 67 | 3 | 13 | 11 |
| 50-100 | 6 | -15 | -3 | 2 | -26 | 42 | -21 | -4 | -8 |
| 100-150 | -33 | 33 | 27 | 7 | -64 | 4 | -15 | 2 | -57 |
| 150-200 | - | - | 92 | 50 | - | -50 | 23 | 21 | - |
| 200-250 | - | - | 80 | 12 | - | -91 | 10 | 4 | - |
| 250-300 | - | - | -16 | -7 | - | -91 | -37 | -22 | - |
| 300-400 | - | - | - | -20 | - | - | -84 | -76 | - |
| >400 | - | - | - | -341 | - | - | -202 | -211 | - |
| Total | 10 | -6 | 5 | -5 | -6 | 9 | -30 | -19 | -2 |

Table 25. Root mean square difference (RMSD) differentiated per biome and per AGB bin for the 2018 map. Colour shading is based the legend shown in Figure 7; column headings are as above.

| | | | | | | | | | |
|---|---|---|---|---|---|---|---|---|---|
| 0-50 | 28 | 12 | 18 | 20 | 9 | 82 | 37 | 28 | 18 |
| 50-100 | 17 | 30 | 27 | 29 | 29 | 75 | 33 | 29 | 21 |
| 100-150 | 38 | 33 | 69 | 65 | 64 | 43 | 48 | 48 | 67 |
| 150-200 | - | - | 143 | 102 | - | 65 | 69 | 98 | - |
| 200-250 | - | - | 146 | 96 | - | 101 | 66 | 62 | - |
| 250-300 | - | - | 85 | 84 | - | 92 | 66 | 44 | - |
| 300-400 | - | - | - | 83 | - | - | 97 | 93 | - |
| >400 | - | - | - | 436 | - | - | 211 | 236 | - |
| Total | 23 | 28 | 39 | 95 | 20 | 69 | 69 | 71 | 27 |

## 3.7. AGB maps intercomparison

In this section we assess the stability of map error among the current three CCI-Biomass AGB products and compare the most recent 2010 and 2017 versions with earlier products, i.e., GlobBiomas 2010 (http://globbiomass.org) and version 1 of the CCI Biomass 2017 product.

### Stability of $AGB_{map} - AGB_{ref}$ differences among the 2010, 2017 and 2018 AGB products

According to the World Meteorological Organization (2011) the user requirement for stability is in general a requirement on the extent to which the error of a product remains constant over a longer period. To assess stability of plot-map differences over the three epochs, Figure 11 shows AGB residuals between harmonized tier 1-3 plot data and mapped AGB aggregated to the 0.1° cell level for each combination of map reference years. Whilst the residuals in 2017 are strongly similar to those in 2018 (bottom row), the 2010 map has many cells for which the residuals differ substantially from those in 2017 and 2018, as can be observed in the top row of Figure 11.

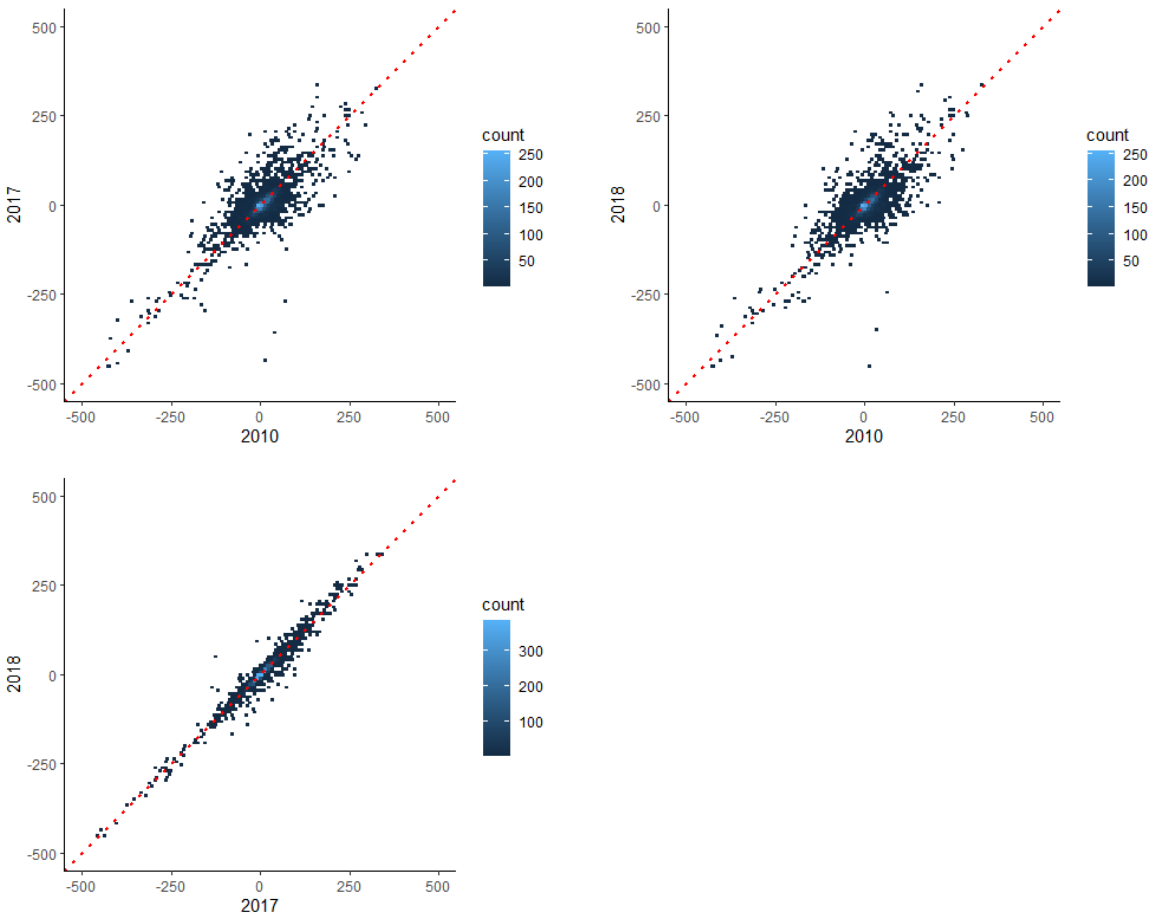


**Figure 11**. AGB residuals between harmonized tier1-3 plot data and mapped AGB at 0.1° cell level for each combination of map reference years. The red dashed line is the 1:1 line.

The map producer may want to know where the largest instabilities in the residuals occur. Such information is provided in Figure 12 where the locations of the 5% most negative differences between the 2010 and 2017 products (2010 – 2017; i.e., points above the 1:1 diagonal in Figure 11) are plotted as red circles whilst the 5% largest positive differences (i.e., points below the 1:1 diagonal) are shown by blue crosses. Several sites have entirely either large positive or large negative differences but in other places, such as east Australia, Madagascar, the northern Balkans and Mexico (Yucatán), both extremes occur close to one another. Figure 13 is a virtually identical figure showing the locations of cells with the most extreme differences between 2010 and 2018 residuals while Figure 14 does so for the 2017 and 2018 residuals. The latter figure has a different pattern of highs and lows but, with additional nearby occurrences of extremes in Gabon.

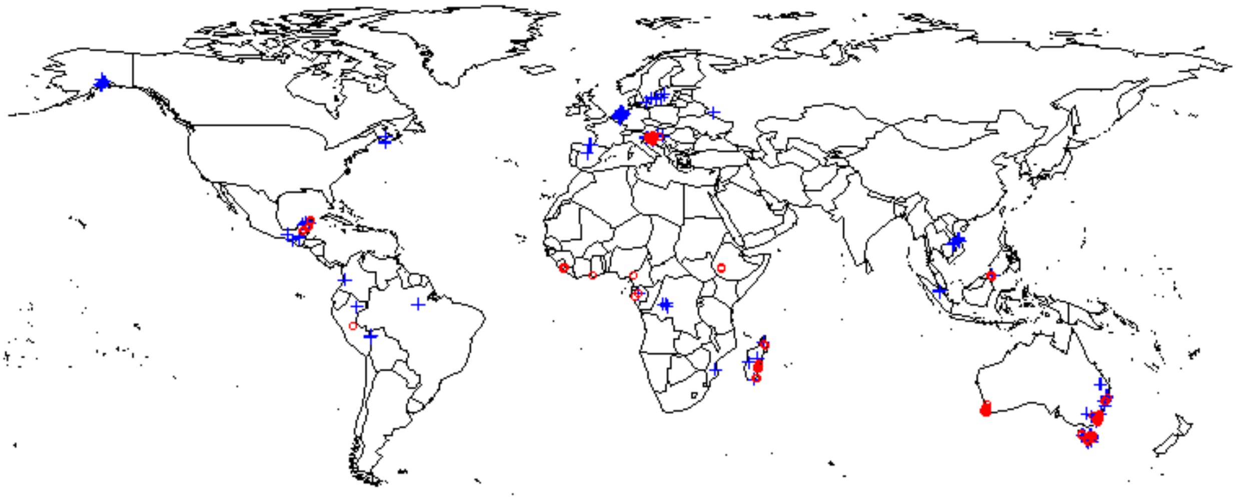

**Figure 12**. Locations of 0.1° cells with the most extreme differences between residuals in the 2010 and 2017 AGB products (2010 – 2017). The 5% cells with the most negative differences (i.e., 2017 > 2010) are indicated in red whilst the 5% largest positive differences (i.e., 2017 < 2010) are shown in blue.

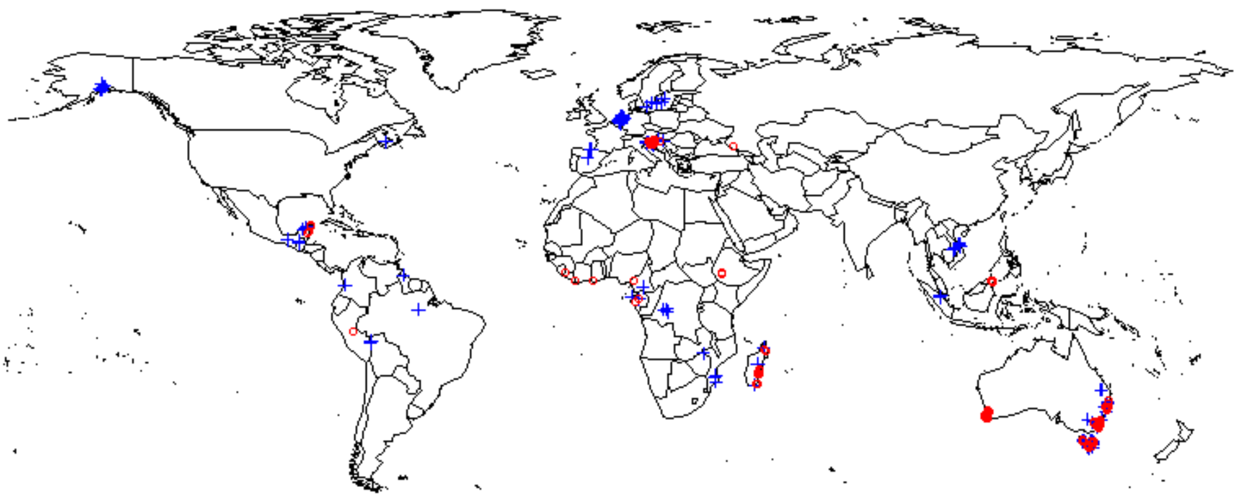

**Figure 13**. Locations of 0.1° cells with the most extreme differences between residuals in the 2010 and 2018 AGB products (2010 – 2018). The 5% cells with the most negative differences (i.e., 2018 > 2010) are indicated in red whilst the 5% largest positive differences (i.e., 2018 < 2010) are shown in blue.

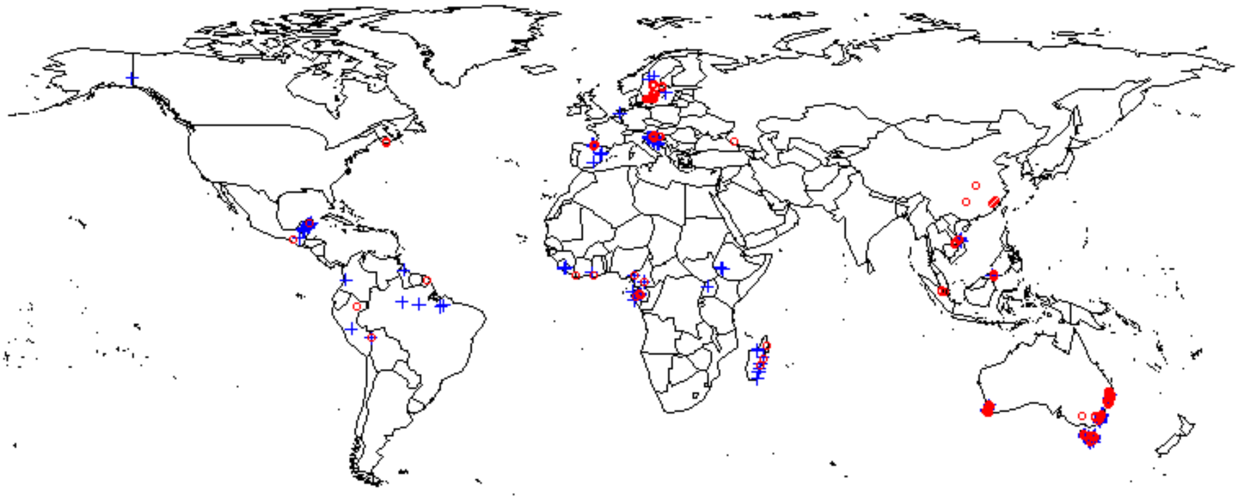

**Figure 14**. Locations of 0.1° cells with the most extreme differences between residuals in the 2017 and 2018 AGB products (2017 – 2018). The 5% cells with the most negative differences (i.e., 2018 > 2017) are indicated in red whilst the 5% largest positive differences (i.e., 2018 < 2017) are shown in blue.

### Comparison of current maps with previous 2010 and 2017 AGB products

Figure 15 shows the global $AGM_{map}$ - $AGB_{ref}$ comparisons spatially aggregated to 0.1° and binned over 25 Mg/ha wide biomass ranges for the GlobBiomass 2010 AGB product against the new CCI Biomass 2010 product and such comparison for versions 1 and 2 of the CCI Biomass 2017 AGB products. Particularly in the highest $AGB_{ref}$ bins, map bias for the higher $AGB_{ref}$ has decreased in the most recent versions but the peaks around $AGB_{ref}$ ≈ 200 Mg/ha discussed earlier need further attention. As mentioned before, this peak arises from a set of plots in east Australia.

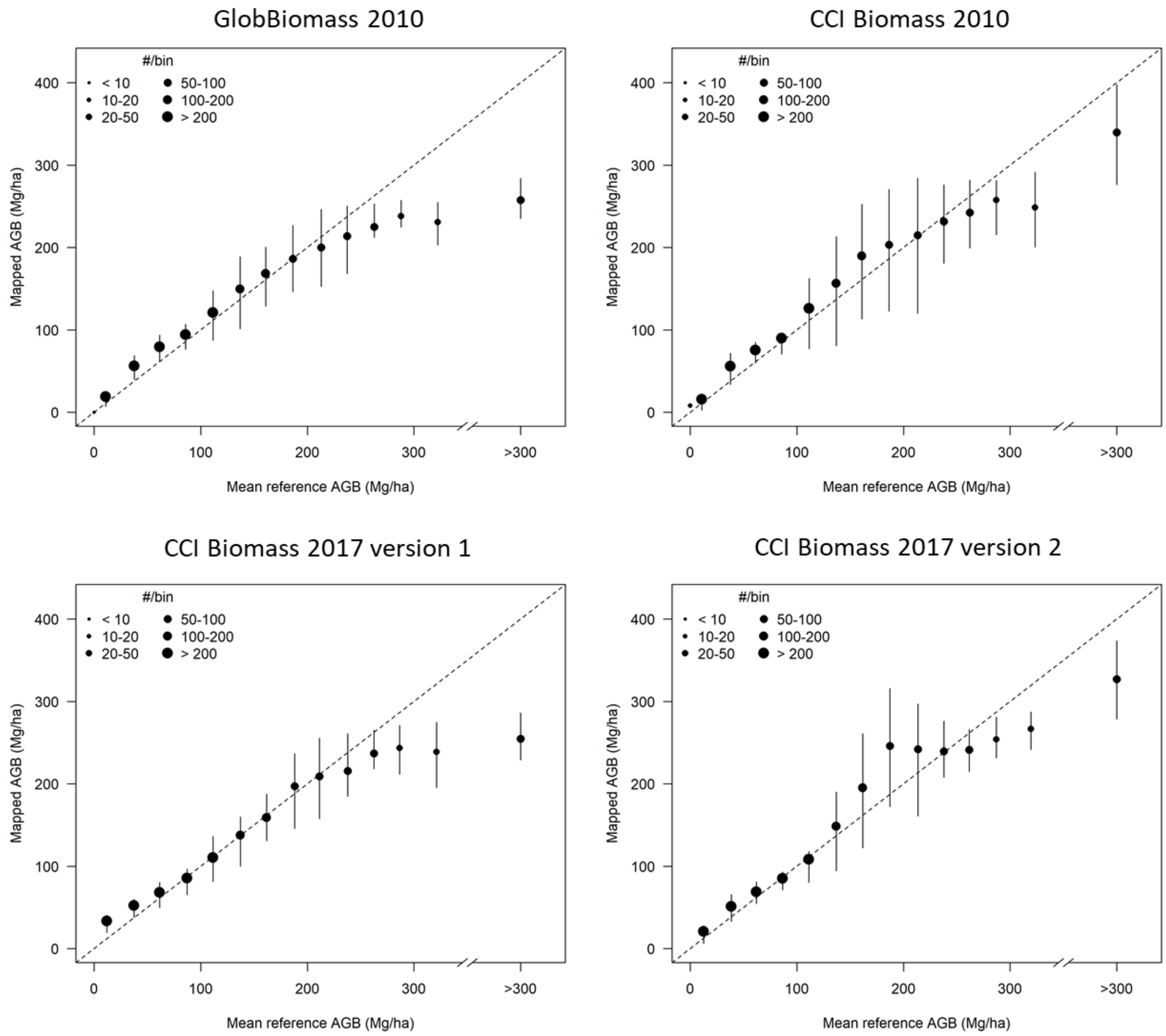


**Figure 15**. Global $AGM_{map}$ - $AGB_{ref}$ comparisons based on inverse variance weighted tier 1-3 plot data spatially aggregated to 0.1° cells.

## 3.8. Within-pixel sampling error

Using the —forest only— LiDAR derived AGB data from forest sites in Remningstorp, Sweden (Ulander et al., 2011), and Lope, Gabon (Hajnsek et al., 2017) the variograms shown in Figure 16 were estimated. The Remningstorp variogram was modelled by two exponential structures with partial sills of 3579 and 1899 $Mg^2/ha^2$ and range parameters of 95 and 531 m, respectively. The Lope variogram was modelled by a 4053 $Mg^2/ha^2$ nugget and a single exponential structure with partial sill of 10553 $Mg^2/ha^2$ and a range parameter of 85 m. Note that the effective range of an exponential variogram is approximately three times the range parameter.

Not surprisingly, the tropical high biomass Lope site has much larger short-range spatial variation than the boreal Remningstorp site (note the different scales on the y-axes).

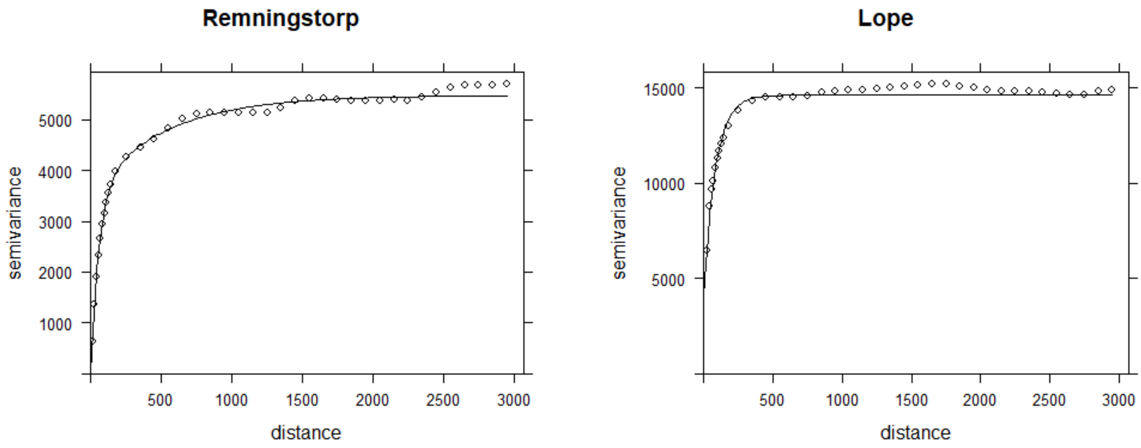


**Figure 16**. Variograms for the Remningstorp and Lope forest sites. Open dots indicate the experimental variogram and the solid lines represent the fitted models.

Based on the variograms and assuming single plots with the size of the LiDAR footprints (i.e., 0.01 ha for Remningstorp and 0.04 ha for Lope) centred in 1ha AGB map pixels, the variance of the plot within pixel sampling error variance was found to be 1421 and 6714 $Mg^2/ha^2$ for the two sites. Hence, the standard deviations amount to 38 and 82 Mg/ha, respectively, which is no negligible.

As demonstrated in the PUG (Santoro, 2020), within-pixel sampling error may suggest map bias even if the map provides a perfect representation of mean AGB at 1 ha spatial support. To replicate this issue using a geostatistical approach, Figure 17 shows a scatterplot of 0.04 ha plot AGB values on the x-axis centred and conditioned on 1 ha pixels that are plotted on the y-axis. The pixel values are in the range 10 to 400 Mg/ha and the plot values are drawn from Gaussian populations with mean given by the pixel value and variance and spatial correlation given by the Lope variogram. Any negative value drawn from a Gaussian population was set to zero.

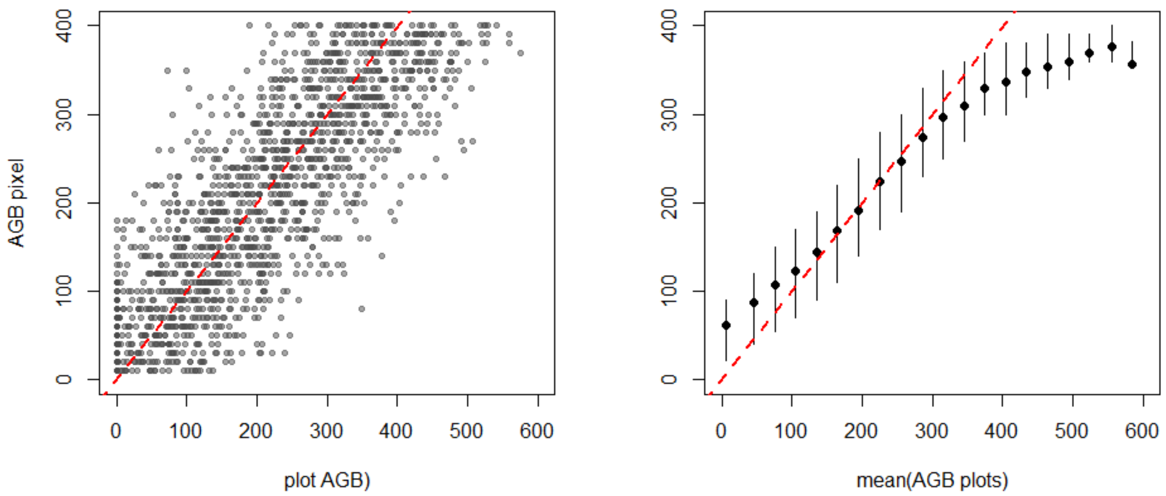


**Figure 17**. Scatterplot of 0.04 ha plot values conditioned on 1 ha pixel values (left) and binned over 30 Mg/ha wide biomass ranges with dots representing mean AGB and whiskers representing the interquartile range of pixel biomass values for plots inside the bins (right). The dashed red lines are 1:1 lines.

The scatter plot and the interquartile whisker plot in Figure 17 suggest the pixel overestimates low AGB and underestimates high AGB at plot level. However, the plot data were conditioned on the pixel data. Therefore, the observed effect is entirely due to the within-pixel sampling error.

The above effect reduces substantially if multiple plots are used to represent a pixel. To demonstrate this, the above experiment was repeated with five plots regularly spread over the pixel. In Figure 18 the means of the AGB from five plots are on the x-axis, while the conditioning pixel values are on the y-axis. In this figure, the bias observed in Figure 17 is mostly absent, except for the far ends of the AGB range.

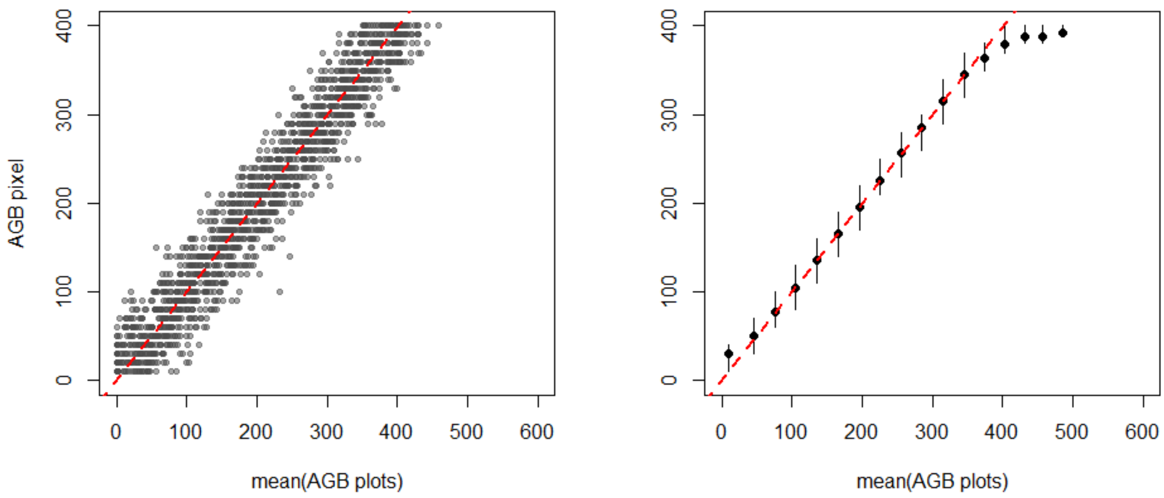


**Figure 18**. Scatterplot of the mean of 0.04 ha plot values conditioned on 1 ha pixel values (left) and binned over 30 Mg/ha wide biomass ranges with dots representing mean AGB and whiskers representing the interquartile range of pixel biomass values (right). The dashed red lines are 1:1 lines.

The reasons for including this section in the PVIR are (1) to corroborate the experiment shown in the PUG (Santoro, 2020) and (2) to demonstrate a method for diagnosing the within-pixel sampling error and show the importance of taking it into account when validating map pixels with data from small plots. For the latter, we need variography for the different environmental circumstances (e.g., biomes), which can be obtained from LiDAR-derived AGB data with small (0.01-0.04 ha) footprint such as the data used in this section. Currently, we have such data only for a single boreal forest site and one site in a tropical forest. More data in these biomes as well as other biomes are needed to routinely account for the within-pixel sampling variance in $AGB_{map}$ – $AGB_{ref}$ comparisons.

# Conclusions

Fully reported and transparent validation is important for increasing acceptance of satellite-derived products in the user community. To assess the accuracy of the AGB estimates of the new 2010, 2017 and 2018 CCI Biomass global maps, AGB predictions were compared with independent plot data, LiDAR-based AGB estimates and recently released CoFor data, which were used as reference data.

The plot data were adjusted for temporal discrepancies and partial forest fraction (see PVP). Three tiers of plot data were defined, ranging from a sizable set (65088 – 118126, depending on the reference year of the AGB map) of data from small plots (on average 0.08 ha), including small NFI plots to a small set of data from large (> 6 ha) research plots (21 – 27). The latter —tier 3— data mainly consist of plots in the tropics that, though of high quality, are so few in number that they barely allow conclusions to be drawn about the quality of the CCI Biomass maps. tier 2 plots (485 - 737), with an average size of 1 ha, revealed that globally the CCI Biomass maps at their original 1 ha resolution tend to over-predict $AGB_{ref}$ up to 200-250 Mg/ha and to under-predict higher $AGB_{ref}$. Similar results were found with the tier 1 data, which builds confidence in using tier 1 plot data for regional accuracy assessments. It should be noted that part of the observed underestimation of high biomass and overestimation of low biomass observed for small plots can be attributed to within-pixel sampling error that occurs because The AGB of single small plots may be significantly differ from the population mean in the pixel.

Spatial aggregation of plot and map data to 0.1° cells (a level of aggregation suitable for most climate modellers) considerably improved the agreement between $AGB_{ref}$ and $AGB_{map}$, though, over-prediction was still observed in the low biomass range and higher reference biomass was under-predicted. Similar results were obtained with LiDAR-based AGB estimates and 1-km pixel Congo basin Forests AGB (CoFor) which suggests their suitability to serve as reference data for assessing global AGB products.

In general, between 50 Mg/ha and 400 Mg/ha, mean differences between $AGB_{map}$ and $AGB_{ref}$ were found to be well within 20% of $AGB_{ref}$ at 0.1° cell level. This does not hold for the RMSD, which over the entire biomass range exceeds 20% of $AGB_{ref}$ for the three maps. Nevertheless, it is concluded that spatial aggregation successfully reduces the effect of localized AGB fluctuations in the map and their potential interaction with plot-map geolocation mismatches. The $AGB_{map}$ - $AGB_{ref}$ comparisons at 0.1° resolution differentiated by biome (Dinerstein et al., 2017) produced patterns similar to the global comparison for many biomes and particularly highlighted confidence in the regional biomass estimations up to 250-300 Mg/ha for the different tropical forest regions. Fits between $AGB_{ref}$ and $AGB_{map}$ were worse for the tropical and subtropical *dry* broadleaf forest biome. Lack of access to a larger set of reference data for this biome may have affected this finding.

The overall analysis at 0.1° cell level revealed that version 2 of the 2017 CCI Biomass AGB map better estimates the high biomass range than version 1. However, we observed overestimation of AGB at $AGB_{ref} \approx 200$ Mg/ha, which was traced to a set of plots in east Australia with widely different AGB densities.

Differences between $AGB_{ref}$ and $AGB_{map}$ were spatially similar in the 2017 and 2018 AGB products. However, the differences were larger when comparing either of those two products with the 2010 AGB product. The locations of the largest differences were mapped to help identifying potential reasons for their occurrence.

This PVIR demonstrated a geostatistical method for assessing the variance of within-pixel sampling error using variography derived from small footprint LiDAR-based AGB estimates from forest sites in Sweden and Gabon. Additional datasets are needed to extend this analysis and use it for error budgeting when using (small) plot data for AGB map assessment.

# Acknowledgements

We are grateful to all data contributors (see Appendix A) for providing forest plot data for the independent validation of the CCI Biomass maps.

# References (including references from Appendix A)

Avitabile, V., Baccini, A., Friedl, M. A., & Schmullius, C. (2012). Capabilities and limitations of Landsat and land cover data for aboveground woody biomass estimation of Uganda. *Remote Sensing of Environment, 117*, 366-380. https://doi.org/10.1016/j.rse.2011.10.012.

Avitabile, V., Schultz, M., Herold, N., de Bruin, S., Pratihast, A. K., Manh, C. P., . . . Herold, M. (2016). Carbon emissions from land cover change in Central Vietnam. *Carbon Management, 7*(5-6), 333-346. doi:10.1080/17583004.2016.1254009

Brown, S., Gillespie, A. J. R., & Lugo, A. E. (1989). Biomass Estimation Methods for Tropical Forests with Applications to Forest Inventory Data. *Forest Science, 35*(4), 881-902. https://doi.org/10.1093/forestscience/35.4.881.

Carreiras, J. M. B., Vasconcelos, M. J., & Lucas, R. M. (2012). Understanding the relationship between aboveground biomass and ALOS PALSAR data in the forests of Guinea-Bissau (West Africa). *Remote Sensing of Environment, 121*, 426-442. https://doi.org/10.1016/j.rse.2012.02.012.

Clark, D. B., & Clark, D. A. (2000). Landscape-scale variation in forest structure and biomass in a tropical rain forest. *Forest Ecology and Management, 137*(1), 185-198. https://doi.org/10.1016/S0378-1127(99)00327-8.

de Bruin, S., Herold, M., & Araza, A. (2019a). *CCI Biomass Product Validation Plan, Year 1, Version 1*. Retrieved from http://cci.esa.int/sites/default/files/biomass%20D2.5%20Product%20Validation%20Plan%20%28PVP%29%20V1.0.pdf.

de Bruin, S., Herold, M., & Araza, A. (2019b). CCI Biomass Product Validation & Intercomparison Report Year 1 Version 1.0. https://climate.esa.int/sites/default/files/biomass_D4.1_Product_Validation_%26_Intercomparison_Report_V1.1.pdf.

de Bruin, S., Herold, M., & Araza, A., Lucas, R. (2020). *CCI Biomass Product Validation Plan, Year 2, Version 2*. https://climate.esa.int/sites/default/files/Biomass_D2.5_Product_Validation_Plan_V2.0.pdf.

DeVries, B., Avitabile, V., Kooistra, L., & Herold, M. (2012). *Monitoring the impact of REDD+ implementation in the Unesco Kafa biosphere reserve, Ethiopia*. Paper presented at the Sensing a Changing World, Wageningen. http://www.wageningenur.nl/upload_mm/9/d/c/f80b6db7-9c3c-4957-8717-6fdc6e46e60f_deVries.pdf.

Dinerstein, E., Olson, D., Joshi, A., Vynne, C., Burgess, N. D., Wikramanayake, E., . . . Saleem, M. (2017). An Ecoregion-Based Approach to Protecting Half the Terrestrial Realm. *BioScience, 67*(6), 534-545. https://doi.org/10.1093/biosci/bix014.

Hajnsek, I., Pardini, M., Jäger, M., Horn, R., Kim, J.S., Jörg, H., Papathanassiou, K., Dubois-Fernandez, P., Dupuis, X., Wasik, V. (2017). Technical Assistance for the Development of Airborne SAR and Geophysical Measurements During the AFRISAR Experiment. Final Report, Deliverable DD-4. pp. 152.

Hansen, M. C., Potapov, P. V., Moore, R., Hancher, M., Turubanova, S. A., Tyukavina, A., . . . Townshend, J. R. G. (2013). High-Resolution Global Maps of 21st-Century Forest Cover Change. *Science, 342*(6160), 850-853. https://doi.org/10.1126/science.1244693.

Hijmans, R. J. (2017). raster: Geographic Data Analysis and Modeling (Version 2.6). Retrieved from https://CRAN.R-project.org/package=raster.

Hirsh, F., Jourget, J. G., Feintrenie, L., Bayol, N., & Ebaá Atyi, R. (2013). *Projet pilote REDD+ de la Lukénie*. Retrieved from Bogor, Indonesia: https://agritrop.cirad.fr/572060/1/document_572060.pdf.

Horn, B. (1981). Hill shading and the reflectance map. *Proceedings of the IEEE, 69*, 14-47. doi:10.1109/PROC.1981.11918

IPPC. (2006). IPCC Guidelines for National Greenhouse Gas Inventories. https://www.ipcc.ch/report/2006-ipcc-guidelines-for-national-greenhouse-gas-inventories/

IPCC. (2019). 2019 Refinement to the 2006 IPCC Guidelines for National Greenhouse Gas Inventories. (table 4.9). https://www.ipcc.ch/report/2019-refinement-to-the-2006-ipcc-guidelines-for-national-greenhouse-gas-inventories/

Kyriakidis, P.C. (2004). A Geostatistical Framework for Area-to-Point Spatial Interpolation. *Geographical Analysis*, 36: 259-289. https://doi.org/10.1111/j.1538-4632.2004.tb01135.x.

Labrière, N., Tao, S., Chave, J., Scipal, K., Toan, T. L., Abernethy, K., . . . Saatchi, S. (2018). In SituReference Datasets From the TropiSAR and AfriSAR Campaigns in Support of Upcoming Spaceborne Biomass Missions. *IEEE Journal of Selected Topics in Applied Earth Observations and Remote Sensing, 11*(10), 3617-3627. doi:10.1109/JSTARS.2018.2851606

Labrière, N., & Chave, J. (2020a) CCI Biomass project – In situ datasets: Processing and validation of Sustainable Landscape Brazil data (CCI Biomass internal report).

Labrière, N., & Chave, J. (2020b) CCI Biomass project – In situ datasets: Processing and validation of NEON data (USA) (CCI Biomass internal report).

Labrière, N., & Chave, J. (2020c) In situ datasets: Processing and validation of TERN data (CCI Biomass internal report).

Lewis, S. L., Sonké, B., Sunderland, T., Begne, S. K., Lopez-Gonzalez, G., van der Heijden, G. M. F., . . . Zemagho, L. (2013). Above-ground biomass and structure of 260 African tropical forests. *Philosophical Transactions of the Royal Society B: Biological Sciences, 368*(1625), 20120295. https://doi.org/10.1098/rstb.2012.0295.

Mello, L. N. C., Sales, M. H. R., & Rosa, L. P. (2016). Analysis of results of biomass forest inventory in northeastern Amazon for development of REDD+ carbon project. *Anais da Academia Brasileira de Ciências, 88*, 55-64.

Mitchard, E. T. A., Saatchi, S. S., Lewis, S. L., Feldpausch, T. R., Gerard, F. F., Woodhouse, I. H., & Meir, P. (2011). Comment on 'A first map of tropical Africa's above-ground biomass derived from satellite imagery'. *Environmental Research Letters, 6*(4), 049001. https://doi.org/10.1088/1748-9326/6/4/049001.

Mitchard, E. T. A., Saatchi, S. S., Woodhouse, I. H., Nangendo, G., Ribeiro, N. S., Williams, M., . . . Meir, P. (2009). Using satellite radar backscatter to predict above-ground woody biomass: A consistent relationship across four different African landscapes. *Geophysical Research Letters, 36*(23). https://doi.org/10.1029/2009gl040692.

Morel, A. C., Saatchi, S. S., Malhi, Y., Berry, N. J., Banin, L., Burslem, D., . . . Ong, R. C. (2011). Estimating aboveground biomass in forest and oil palm plantation in Sabah, Malaysian Borneo using ALOS PALSAR data. *Forest Ecology and Management, 262*(9), 1786-1798. https://doi.org/10.1016/j.foreco.2011.07.008.

Paul, K. I., Roxburgh, S. H., Chave, J., England, J. R., Zerihun, A., Specht, A., . . . Sinclair, J. (2016). Testing the generality of above-ground biomass allometry across plant functional types at the continent scale. *Global Change Biology, 22*(6), 2106-2124. https://doi.org/10.1111/gcb.13201.

Pebesma, E.J. (2004). Multivariable geostatistics in S: the gstat package. Computers & Geosciences, 30: 683-691.

Ploton, P., Mortier, F., Barbier, N. et al. (2020). A map of African humid tropical forest aboveground biomass derived from management inventories. Sci Data 7, 221. https://doi.org/10.1038/s41597-020-0561-0.

Réjou-Méchain, M., Barbier, N., Couteron, P., Ploton, P., Vincent, G., Herold, M., . . . Pélissier, R. (2019). Upscaling Forest Biomass from Field to Satellite Measurements: Sources of Errors and Ways to Reduce Them. *Surveys in Geophysics*. https://doi.org/10.1007/s10712-019-09532-0.

Réjou-Méchain, M., Muller-Landau, H. C., Detto, M., Thomas, S. C., Le Toan, T., Saatchi, S. S., . . . Chave, J. (2014). Local spatial structure of forest biomass and its consequences for remote sensing of carbon stocks. *Biogeosciences, 11*(23), 6827-6840. https://doi.org/10.5194/bg-11-6827-2014.

Réjou-Méchain, M., Tanguy, A., Piponiot, C., Chave, J., & Hérault, B. (2017). biomass: an r package for estimating above-ground biomass and its uncertainty in tropical forests. *Methods in Ecology and Evolution, 8*(9), 1163-1167. https://doi.org/10.1111/2041-210X.12753.

Requena Suarez, D., Rozendaal, D. M. A., De Sy, V., Phillips, O. L., Alvarez-Dávila, E., Anderson-Teixeira, K., . . . Herold, M. (2019). Estimating aboveground net biomass change for tropical and subtropical forests: Refinement of IPCC default rates using forest plot data. *Global Change Biology, 25*(11), 3609-3624. doi:10.1111/gcb.14767

Rozendaal, D. M. A., M. Santoro, D. Schepaschenko, V. Avitabile and M. Herold (2017). DUE GlobBiomass D17 Validation Report, European Space Agency (ESA-ESRIN): 26.

Ryan, C. M., Berry, N. J., & Joshi, N. (2014). Quantifying the causes of deforestation and degradation and creating transparent REDD+ baselines: A method and case study from central Mozambique. *Applied Geography, 53*, 45-54. https://doi.org/10.1016/j.apgeog.2014.05.014.

Santoro, M., 2020. *CCI Biomass Product User Guide, Year 2, Version 2*. (CCI Biomass internal report).

Schepaschenko, D., Chave, J., Phillips, O. L., Lewis, S. L., Davies, S. J., Réjou-Méchain, M., . . . Zo-Bi, I. C. (2019). The Forest Observation System, building a global reference dataset for remote sensing of forest biomass. *Scientific Data, 6*(1), 198. https://doi.org/10.1038/s41597-019-0196-1.

Ulander, L.M.H., Gustavsson, A., Flood, B., Murdin, D., Dubois-Fernandez, P., Dupuis, X., Sandberg, G., Soja, M.J., Eriksson, L.E.B., Fransson, J.E.S., Holmgren, J., Wallerman, J. (2011). BioSAR 2010 - Technical assistance for the development of airborne SAR and geophysical measurements during the BioSAR 2010 experiment.

Vaglio Laurin, G., Hawthorne, W., Chiti, T., Di Paola, A., Cazzolla Gatti, R., Marconi, S., . . . Valentini, R. (2016). Does degradation from selective logging and illegal activities differently impact forest resources? A case study in Ghana. [Does degradation from selective logging and illegal activities differently impact forest resources? A case study in Ghana]. *iForest - Biogeosciences and Forestry, 9*(3), 354-362. https://doi.org/10.3832/ifor1779-008.

Van Breugel, M., Bongers, F., & Martínez-Ramos, M. (2007). Species Dynamics During Early Secondary Forest Succession: Recruitment, Mortality and Species Turnover. *Biotropica, 39*(5), 610-619. https://doi.org/10.1111/j.1744-7429.2007.00316.x.

Vieilledent, G., Gardi, O., Grinand, C., Burren, C., Andriamanjato, M., Camara, C., . . . Rakotoarijaona, J.-R. (2016). Bioclimatic envelope models predict a decrease in tropical forest carbon stocks with climate change in Madagascar. *Journal of Ecology, 104*(3), 703-715. https://doi.org/10.1111/1365-2745.12548.

Willcock, S., Phillips, O. L., Platts, P. J., Balmford, A., Burgess, N. D., Lovett, J. C., . . . Lewis, S. L. (2014). Quantifying and understanding carbon storage and sequestration within the Eastern Arc Mountains of Tanzania, a tropical biodiversity hotspot. *Carbon Balance and Management, 9*(1), 2. https://doi.org/10.1186/1750-0680-9-2.

World Meteorological Organization (2011). Systematic observation requirements for satellite-based data products for climate: Supplemental details to the satellite-based component of the Implementation Plan for the Global Observing System for Climate in Support of the UNFCCC (2010 Update). https://library.wmo.int/doc_num.php?explnum_id=3710.

# Appendix A - Details on the used forest plot data

| ID | Tier | Average year | Average size (ha) | Count | Biome | URL | Paper/ source | Data access |
|---|---|---|---|---|---|---|---|---|
| AFR_L | 3 | 2011 | 25.00 | 1 | Tropical rainforest | https://dspace.stir.ac.uk/retrieve/74d3b352-fa46-418f-ba95-728bb33f4cfc/08417912.pdf | (Labrière et al., 2018) | open |
| EU_FOS | 3 | 2014 | 16.25 | 1 | Tropical rainforest | https://www.-ture.com/articles/s41597-019-0196-1?fbclid=IwAR08vLoOm4xEQo4EUdLtoKsnP6nsNIY5CYnfcoqGcS5Z0_UcyaNIr-jcdDg | (Schepaschenko et al., 2019) | open |
| SAM_L | 3 | 2010 | 7.65 | 20 | Tropical rainforest | https://dspace.stir.ac.uk/retrieve/74d3b352-fa46-418f-ba95-728bb33f4cfc/08417912.pdf | (Labrière et al., 2018) | open |
| AUS1 | 3 | 2009 | 25.00 | 1 | Tropical dry forest | http://data.auscover.org.au/xwiki/bin/view/Product+pages/Biomass+Plot+Library | (Paul et al., 2016) | source-WUR agreement |
| SAM_RF | 3 | 2008 | 5.3 | 10 | Tropical rainforest | http://www.rainfor.org/en/project/about-rainfor | Lopez-Gonzales et al., 2011 | Open |
| AFR_FOS | 2 | 2013 | 1.00 | 44 | Tropical rainforest | https://www.-ture.com/articles/s41597-019-0196-1?fbclid=IwAR08vLoOm4xEQo4EUdLtoKsnP6nsNIY5CYnfcoqGcS5Z0_UcyaNIr-jcdDg | (Schepaschenko et al., 2019) | open |
| AFR_L | 2 | 2016 | 1.00 | 56 | Tropical rainforest | https://dspace.stir.ac.uk/retrieve/74d3b352-fa46-418f-ba95-728bb33f4cfc/08417912.pdf | (Labrière et al., 2018) | open |
| AUS_FOS | 2 | 2008 | 1.00 | 2 | Tropical dry forest | https://www.-ture.com/articles/s41597-019-0196-1?fbclid=IwAR08vLoOm4xEQo4EUdLtoKsnP6nsNIY5CYnfcoqGcS5Z0_UcyaNIr-jcdDg | (Schepaschenko et al., 2019) | open |
| CAM_FOS | 2 | 2012 | 1.01 | 18 | Tropical rainforest | https://www.-ture.com/articles/s41597-019-0196-1?fbclid=IwAR08vLoOm4xEQo4EUdLtoKsnP6nsNIY5CYnfcoqGcS5Z0_UcyaNIr-jcdDg | (Schepaschenko et al., 2019) | open |
| EU_FOS | 2 | 2010 | 2.23 | 2 | Boreal coniferous forest | https://www.-ture.com/articles/s41597-019-0196-1?fbclid=IwAR08vLoOm4xEQo4EUdLtoKsnP6nsNIY5CYnfcoqGcS5Z0_UcyaNIr-jcdDg | (Schepaschenko et al., 2019) | open |
| SAM_FOS | 2 | 2011 | 1.00 | 23 | Tropical rainforest | https://www.-ture.com/articles/s41597-019-0196-1?fbclid=IwAR08vLoOm4xEQo4EUdLtoKsnP6nsNIY5CYnfcoqGcS5Z0_UcyaNIr-jcdDg | (Schepaschenko et al., 2019) | open |
| SAM_L | 2 | 2013 | 1.04 | 28 | Tropical rainforest | https://dspace.stir.ac.uk/retrieve/74d3b352-fa46-418f-ba95-728bb33f4cfc/08417912.pdf | (Labrière et al., 2018) | open |

| | | | | | | | | |
|---|---|---|---|---|---|---|---|---|
| SAM_BAJ | 2 | 2017 | 1 | 3 | Tropical rainforest | https://ieeexplore.ieee.org/abstract/document/8518871 | Pacheco-Pasccagaza et al., 2020 | source-WUR agreement |
| SAM_RF | 2 | 2008 | 1 | 374 | Tropical rainforest | http://www.rainfor.org/en/project/about-rainfor | Lopez-Gonzales et al., 2011 | Open |
| UK_FOS | 2 | 2015 | 1.20 | 1 | Tropical rainforest | https://www.-ture.com/articles/s41597-019-0196-1?fbclid=IwAR08vLoOm4xEQo4EUdLtoKsnP6nsNIY5CYnfcoqGcS5Z0_UcyaNIr-jcdDg | (Schepaschenko et al., 2019) | open |
| AFR10 | 2 | 2007 | 1.00 | 7 | Tropical rainforest | https://iopscience.iop.org/article/10.1088/1748-9326/6/4/049001/meta | (Mitchard et al., 2011) | source-WUR agreement |
| AFR13 | 2 | 2008 | 1.00 | 2 | Tropical rainforest | https://agupubs.onlinelibrary.wiley.com/doi/full/10.1029/2009GL040692 | (Mitchard et al., 2009) | source-WUR agreement |
| AFR14 | 2 | 2009 | 1.63 | 4 | Tropical rainforest | https://www.sciencedirect.com/science/article/abs/pii/S014362281400109X | (Ryan, Berry, & Joshi, 2014) | source-WUR agreement |
| AFR6 | 2 | 2009 | 1.00 | 12 | Tropical rainforest | https://cbmjour-l.biomedcentral.com/articles/10.1186/1750-0680-9-2 | (Willcock et al., 2014) | source-WUR agreement |
| AFR7 | 2 | 2012 | 1.00 | 19 | Tropical rainforest | https://royalsocietypublishing.org/doi/full/10.1098/rstb.2012.0295 | (Lewis et al., 2013) | source-WUR agreement |
| ASI3 | 2 | 2007 | 1.00 | 92 | Tropical rainforest | https://www.sciencedirect.com/science/article/abs/pii/S0378112711004361 | (Morel et al., 2011) | source-WUR agreement |
| AUS1 | 2 | 2012 | 1.01 | 63 | Subtropical steppe | http://data.auscover.org.au/xwiki/bin/view/Product+pages/Biomass+Plot+Library | (Paul et al., 2016) | source-WUR agreement |
| SAM2 | 2 | 2012 | 1.00 | 40 | Tropical rainforest | http://geoinfo.cnpm.embrapa.br/geonetwork/srv/ eng/main.home | | source-WUR agreement |
| SAM_FOS | 1 | 2011 | 0.25 | 142 | Tropical rainforest | https://www.-ture.com/articles/s41597-019-0196-1?fbclid=IwAR08vLoOm4xEQo4EUdLtoKsnP6nsNIY5CYnfcoqGcS5Z0_UcyaNIr-jcdDg | (Schepaschenko et al., 2019) | open |
| AFR15 | 1 | 2013 | 0.25 | 136 | Tropical rainforest | https://besjour-ls.onlinelibrary.wiley.com/doi/full/10.1111/1365-2745.12548%4010.1111/%28ISSN%291365-2745.FORESTRY | (Vieilledent et al., 2016) | source-WUR agreement |
| AFR1 | 1 | 2008 | 0.50 | 1152 | Tropical rainforest | https://agritrop.cirad.fr/572060/1/document_572060.pdf | (Hirsh, Jourget, Feintrenie, Bayol, | source-WUR |

| | | | | | | | | |
|---|---|---|---|---|---|---|---|---|
| | | | | | | | & Ebaá Atyi, 2013) | agreement |
| AFR10 | 1 | 2007 | 0.50 | 11 | Tropical rainforest | https://iopscience.iop.org/article/10.1088/1748-9326/6/4/049001/meta | (Mitchard et al., 2011) | source-WUR agreement |
| AFR12 | 1 | 2008 | 0.16 | 108 | Tropical rainforest | https://www.sciencedirect.com/science/article/abs/pii/S0034425711003609 | (Avitabile, Baccini, Friedl, & Schmullius, 2012) | source-WUR agreement |
| AFR13 | 1 | 2008 | 0.50 | 23 | Tropical rainforest | https://agupubs.onlinelibrary.wiley.com/doi/full/10.1029/2009GL040692 | (Mitchard et al., 2009) | source-WUR agreement |
| AFR14 | 1 | 2009 | 0.51 | 70 | Tropical dry forest | https://www.sciencedirect.com/science/article/abs/pii/S014362281400109X | (Ryan et al., 2014) | source-WUR agreement |
| AFR4 | 1 | 2012 | 0.13 | 110 | Tropical mountain system | http://www.geo-informatie.nl/workshops/scw2/papers/deVries.pdf | (DeVries, Avitabile, Kooistra, & Herold, 2012) | source-WUR agreement |
| AFR5 | 1 | 2012 | 0.08 | 71 | Tropical rainforest | https://pure.mpg.de/pubman/faces/ViewItemOverviewPage.jsp?itemId=item_2281402 | (Vaglio Laurin et al., 2016) | source-WUR agreement |
| AFR6 | 1 | 2009 | 0.33 | 12 | Tropical dry forest | https://cbmjour-l.biomedcentral.com/articles/10.1186/1750-0680-9-2 | (Willcock et al., 2014) | source-WUR agreement |
| AFR8 | 1 | 2008 | 0.13 | 105 | Tropical moist forest | https://www.sciencedirect.com/science/article/abs/pii/S0034425712001058 | (Carreiras, Vasconcelos, & Lucas, 2012) | source-WUR agreement |
| AFR9 | 1 | 2016 | 0.13 | 9642 | Tropical dry forest | https://www.mdpi.com/2072-4292/5/4/1524<br>https://fndsmoz.maps.arcgis.com/apps/MapSeries/index.html?appid=6602939f39ad4626a10f87bf6253af1e | (Carreiras et al., 2012) | open, source-WUR agreement |
| AFR_KEN | 1 | 2011 | 0.09 | 362 | Tropical and subtropical grasslands, savannas and shrublands | | | source-WUR agreement |
| ASI1 | 1 | 2008 | 0.05 | 2903 | Tropical mountain system and rainforest | https://www.tandfonline.com/doi/full/10.1080/17583004.2016.1254009 | (Avitabile et al., 2016) | source-WUR agreement |

| | | | | | | | | |
|---|---|---|---|---|---|---|---|---|
| ASI10 | 1 | 2008 | 0.10 | 1268 | Subtropical mountain system | https://www.sciencedirect.com/science/article/abs/pii/S0034425719303608 | Zhang et al. 2019 | source-WUR agreement |
| ASI2 | 1 | 2011 | 0.11 | 119 | Tropical dry forest | http://www.leafasia.org/sites/default/files/public/resources/WWF-REDD-pres-July-2013-v3.pdf | WWF and OBf, 2013 | source-WUR agreement |
| ASI4 | 1 | 2010 | 0.02 | 70 | Tropical dry forest | http://citeseerx.ist.psu.edu/viewdoc/download?doi=10.1.1.972.708&rep=rep1&type=pdf | Wijaya et al., 2015 | source-WUR agreement |
| ASI9 | 1 | 2012 | 0.13 | 74 | Tropical rainforest | http://leutra.geogr.uni-je-.de/vgtbRBIS/metadata/start.php | Avitabile et al., 2014 | source-WUR agreement |
| ASI_FOS | 1 | 2014 | 0.25 | 2 | Tropical rainforest | https://www.-ture.com/articles/s41597-019-0196-1?fbclid=IwAR08vLoOm4xEQo4EUdLtoKsnP6nsNIY5CYnfcoqGcS5Z0_UcyaNIr-jcdDg | (Schepaschenko et al., 2019) | open |
| AUS1 | 1 | 2011 | 0.12 | 5611 | Tropical dry forest | http://data.auscover.org.au/xwiki/bin/view/Product+pages/Biomass+Plot+Library | Paul et al. 2016 | source-WUR agreement |
| EU1 | 1 | 2011 | 0.01 | 16819 | Temperate broadleaf and mixed forests and Boreal forests | https://www.slu.se/en/collaborative-centres-and-projects/swedish--tio-l-forest-inventory/ | Sweden NFI | source-WUR agreement |
| EU2 | 1 | 2007 | 0.20 | 7177 | Mediterranean forests | http://www.magrama.gob.es/es/desarrollo-rural/temas/politica-forestal/inventario-cartografia/inventario-forestal--cio-l/ | Spain NFI | source-WUR agreement |
| EU3 | 1 | 2013 | 0.06 | 3021 | Temperate oceanic forest | https://library.wur.nl/WebQuery/wurpubs/454875 | Netherlands NFI | source-WUR agreement |
| EU4 | 1 | 2007 | 0.06 | 5967 | Temperate broadleaf and mixed forests and Mediterranean forests | https://www.agriculturejour-ls.cz/publicFiles/01003.pdf | Cienciela et al. 2008 | source-WUR agreement |
| EU_FOS | 1 | 2015 | 0.28 | 514 | Boreal forests | https://www.-ture.com/articles/s41597-019-0196-1?fbclid=IwAR08vLoOm4xEQo4EUdLtoKsnP6nsNIY5CYnfcoqGcS5Z0_UcyaNIr-jcdDg | (Schepaschenko et al., 2019) | open, source-WUR agreement |
| NAM1 | 1 | 2010 | 0.04 | 586 | Boreal coniferous forest | https://www.p-s.org/content/112/18/5738.short | Liang et al., 2015 | source-WUR agreement |
| NAM2 | 1 | 2004 | 0.04 | 75 | Temperate mountain system | https://www.nature.com/articles/nature07276 | Luyssaert et al., 2008 | source-WUR agreement |

| | | | | | | | | |
|---|---|---|---|---|---|---|---|---|
| NAM3 | 1 | 2010 | 0.03 | 588 | Temperate continental forest | | | source-WUR agreement |
| NAM4 | 1 | 2010 | 0.04 | 2794 | Temperate mountain system | | Alaska NFI | source-WUR agreement |
| SAM2 | 1 | 2013 | 0.23 | 241 | Tropical rainforest | https://www.paisagenslidar.cnptia.embrapa.br/webgis/ | Embrapa, undated | source-WUR agreement |
| SAM3 | 1 | 2011 | 0.13 | 111 | Tropical rainforest | | CIFOR, undated | source-WUR agreement |
| SAM4 | 1 | 2014 | 0.15 | 7 | Tropical rainforest | | CIFOR, undated | source-WUR agreement |
| SAM5 | 1 | 2014 | 0.60 | 23 | Tropical rainforest | | CIFOR, undated | source-WUR agreement |
| SAM_BAJ | 1 | 2017 | 0.25 | 363 | Tropical rainforest | https://ieeexplore.ieee.org/abstract/document/8518871 | Pacheco-Pasccagaza et al., 2020 | source-WUR agreement |
| SAM_RF | 1 | 2008 | 1 | 125 | Tropical rainforest | http://www.rainfor.org/en/project/about-rainfor | Lopez-Gonzales et al., 2011 | Open |
| SAM_TAPA | 1 | 2009 | 0.5 | 138 | Tropical rainforest | https://www.tandfonline.com/doi/full/10.1080/07038992.2014.913477?casa_token=EZxeZoegekkAAAAA%3AZHCN98XtpZRrsS9KoGTBhPy1_yzhAkkLZHfck3fomwSnvSaO7YDiuPV_hne6Mj1Wdn-7ME_sPChP | (Bispo et al., 2014) | source-WUR agreement |
| AFR_COF | 0 | 2009 | 100 | 35029 | Tropical moist forest, | https://www.nature.com/articles/s41597-020-0561-0 | (Ploton et al., 2020) | open |
| LIDAR | 0 | 2014 | 1 | 744397 | Tropical rainforest | | SLB, TERN, NEON | open |

# Appendix B – Tables of assessments per biome

Table 26. Validation results for the boreal forests biome based on spatially aggregated data of all tiers, LiDAR-based and CoFor AGB data.

| | | 2010 | | | | 2017 | | | | | 2018 | | | | |
|---|---|---|---|---|---|---|---|---|---|---|---|---|---|---|---|
| $AGB_{ref}$ bin [Mg/ha] | # cells count | $AGB_{ref}$ | $AGB_{map}$ | $MD$ | $RMSD$ | # cells count | $AGB_{ref}$ | $AGB_{map}$ | $MD$ | $RMSD$ | # cells count | $AGB_{ref}$ | $AGB_{map}$ | $MD$ | $RMSD$ |
| | | ------------------[Mg/ha] ---------------- | | | | | -----------------[Mg/ha] -------------- | | | | | -------------------[Mg/ha] ------------- | | | |
| 0-50 | 531 | 34 | 64 | 30 | 32 | 418 | 37 | 63 | 26 | 29 | 418 | 37 | 61 | 24 | 28 |
| 50-100 | 494 | 68 | 75 | 7 | 16 | 572 | 69 | 76 | 7 | 17 | 572 | 69 | 75 | 6 | 17 |
| 100-150 | 49 | 115 | 77 | -38 | 40 | 69 | 115 | 82 | -33 | 37 | 69 | 115 | 82 | -33 | 38 |
| total | 1074 | 54 | 70 | 16 | 27 | 1059 | 60 | 71 | 12 | 24 | 1059 | 60 | 70 | 10 | 23 |

Table 27. Validation results for the mangroves biome based on spatially aggregated data of all tiers, LiDAR-based and CoFor AGB data.

| | | 2010 | | | | 2017 | | | | | 2018 | | | | |
|---|---|---|---|---|---|---|---|---|---|---|---|---|---|---|---|
| $AGB_{ref}$ bin [Mg/ha] | # cells count | $AGB_{ref}$ | $AGB_{map}$ | $MD$ | $RMSD$ | # cells count | $AGB_{ref}$ | $AGB_{map}$ | $MD$ | $RMSD$ | # cells count | $AGB_{ref}$ | $AGB_{map}$ | $MD$ | $RM$ |
| | | ------------------[Mg/ha] ----------------- | | | | | ---------------------[Mg/ha] ---------------- | | | | | -------------------[Mg/ha] ----------- | | | |
| 0-50 | 10 | 34 | 55 | 21 | 47 | 4 | 36 | 46 | 10 | 12 | 4 | 36 | 46 | 10 | |
| 50-100 | 8 | 62 | 47 | -14 | 26 | 13 | 70 | 54 | -16 | 31 | 13 | 70 | 55 | -15 | |
| 100-150 | 1 | 100 | 164 | 64 | 64 | 1 | 119 | 155 | 35 | 35 | 1 | 119 | 153 | 33 | |
| total | 19 | 49 | 57 | 9 | 41 | 18 | 65 | 58 | -7 | 29 | 18 | 65 | 59 | -6 | |

Table 28. Validation results for the Mediterranean forests, woodland and scrub biome based on spatially aggregated data of all tiers, LiDAR-based and CoFor AGB data.

| | 2010 | | | | | 2017 | | | | | 2018 | | | | |
|---|---|---|---|---|---|---|---|---|---|---|---|---|---|---|---|
| $AGB_{ref}$ bin [Mg/ha] | # cells count | $AGB_{ref}$ | $AGB_{map}$ | *MD* | *RMSD* | # cells count | $AGB_{ref}$ | $AGB_{map}$ | *MD* | *RMSD* | # cells count | $AGB_{ref}$ | $AGB_{map}$ | *MD* | *RMSD* |
| | | [Mg/ha] | | | | | [Mg/ha] | | | | | [Mg/ha] | | | |
| 0-50 | 2518 | 17 | 18 | 1 | 15 | 886 | 20 | 23 | 3 | 19 | 886 | 20 | 20 | 0 | 18 |
| 50-100 | 292 | 64 | 78 | 14 | 37 | 136 | 65 | 66 | 1 | 27 | 136 | 65 | 62 | -3 | 27 |
| 100-150 | 40 | 127 | 161 | 34 | 101 | 28 | 126 | 151 | 26 | 69 | 28 | 126 | 152 | 27 | 69 |
| 150-200 | 29 | 171 | 197 | 26 | 94 | 31 | 170 | 260 | 90 | 137 | 31 | 170 | 263 | 92 | 143 |
| 200-250 | 26 | 224 | 217 | -7 | 87 | 23 | 222 | 298 | 76 | 133 | 23 | 222 | 302 | 80 | 146 |
| 250-300 | 8 | 273 | 238 | -36 | 91 | 7 | 270 | 249 | -21 | 84 | 7 | 270 | 254 | -16 | 85 |
| 300-400 | 3 | 304 | 219 | -85 | 96 | 3 | 304 | 344 | 40 | 90 | 3 | 304 | 380 | 77 | 138 |
| total | 2916 | 28 | 30 | 3 | 26 | 1114 | 39 | 46 | 7 | 38 | 1114 | 39 | 44 | 5 | 39 |

Table 29. Validation results for the temperate broadleaf and mixed forests biome based on spatially aggregated data of all tiers, LiDAR-based and CoFor AGB data.

| | 2010 | | | | | 2017 | | | | | 2018 | | | | |
|---|---|---|---|---|---|---|---|---|---|---|---|---|---|---|---|
| $AGB_{ref}$ bin [Mg/ha] | # cells count | $AGB_{ref}$ | $AGB_{map}$ | *MD* | *RMSD* | # cells count | $AGB_{ref}$ | $AGB_{map}$ | *MD* | *RMSD* | # cells count | $AGB_{ref}$ | $AGB_{map}$ | *MD* | *RMSD* |
| | | [Mg/ha] | | | | | [Mg/ha] | | | | | [Mg/ha] | | | |
| 0-50 | 388 | 38 | 67 | 30 | 37 | 180 | 39 | 45 | 7 | 20 | 180 | 39 | 44 | 5 | 20 |
| 50-100 | 821 | 72 | 83 | 11 | 35 | 763 | 76 | 78 | 2 | 29 | 764 | 76 | 78 | 2 | 29 |
| 100-150 | 307 | 121 | 148 | 27 | 90 | 328 | 119 | 124 | 5 | 63 | 328 | 119 | 126 | 7 | 65 |
| 150-200 | 114 | 171 | 208 | 37 | 100 | 92 | 173 | 221 | 48 | 99 | 92 | 173 | 223 | 50 | 102 |
| 200-250 | 43 | 224 | 225 | 0 | 99 | 38 | 223 | 235 | 12 | 93 | 38 | 223 | 235 | 12 | 96 |
| 250-300 | 24 | 277 | 238 | -39 | 102 | 21 | 271 | 258 | -13 | 77 | 21 | 271 | 263 | -7 | 84 |
| 300-400 | 23 | 349 | 316 | -33 | 96 | 22 | 348 | 327 | -21 | 77 | 22 | 348 | 328 | -20 | 83 |
| >400 | 48 | 698 | 366 | -333 | 429 | 52 | 688 | 347 | -341 | 436 | 52 | 688 | 347 | -341 | 436 |
| total | 1768 | 107 | 115 | 9 | 92 | 1496 | 119 | 112 | -6 | 95 | 1497 | 118 | 113 | -5 | 95 |

Table 30. Validation results for the temperate grasslands, savannas and shrublands biome based on spatially aggregated data of all tiers, LiDAR-based and CoFor AGB data.

| | | | 2010 | | | | | 2017 | | | | | 2018 | | |
|---|---|---|---|---|---|---|---|---|---|---|---|---|---|---|---|
| $AGB_{ref}$ bin | # cells | $AGB_{ref}$ | $AGB_{map}$ | *MD* | *RMSD* | # cells | $AGB_{ref}$ | $AGB_{map}$ | *MD* | *RMSD* | # cells | $AGB_{ref}$ | $AGB_{map}$ | *MD* | *RMSD* |
| [Mg/ha] | count | ------------------[Mg/ha] ----------------- | | | | count | ---------------------[Mg/ha] ---------------- | | | | count | -------------------[Mg/ha] -------------- | | | |
| 0-50 | 48 | 16 | 26 | 10 | 25 | 18 | 14 | 16 | 2 | 8 | 18 | 14 | 16 | 2 | 9 |
| 50-100 | 15 | 75 | 92 | 17 | 55 | 4 | 67 | 36 | -31 | 33 | 4 | 67 | 41 | -26 | 29 |
| 100-150 | 9 | 112 | 153 | 41 | 89 | 1 | 150 | 94 | -56 | 56 | 1 | 150 | 86 | -64 | 64 |
| 150-200 | 1 | 191 | 168 | -23 | 23 | | | | | | | | | | |
| total | 73 | 43 | 57 | 15 | 45 | 23 | 29 | 23 | -7 | 20 | 23 | 29 | 23 | -6 | 20 |

Table 31. Validation results for the tropical and subtropical dry broadleaf forest biome based on spatially aggregated data of all tiers, LiDAR-based and CoFor AGB data.

| | | | 2010 | | | | | 2017 | | | | | 2018 | | |
|---|---|---|---|---|---|---|---|---|---|---|---|---|---|---|---|
| $AGB_{ref}$ bin | # cells | $AGB_{ref}$ | $AGB_{map}$ | *MD* | *RMSD* | # cells | $AGB_{ref}$ | $AGB_{map}$ | *MD* | *RMSD* | # cells | $AGB_{ref}$ | $AGB_{map}$ | *MD* | *RMSD* |
| [Mg/ha] | count | ------------------[Mg/ha] ----------------- | | | | count | ---------------------[Mg/ha] ---------------- | | | | count | -------------------[Mg/ha] -------------- | | | |
| 0-50 | 27 | 30 | 138 | 108 | 120 | 15 | 39 | 116 | 76 | 84 | 15 | 39 | 107 | 67 | 82 |
| 50-100 | 38 | 74 | 124 | 50 | 73 | 28 | 80 | 133 | 53 | 76 | 28 | 80 | 122 | 42 | 75 |
| 100-150 | 24 | 120 | 148 | 27 | 61 | 34 | 118 | 140 | 21 | 42 | 34 | 118 | 122 | 4 | 43 |
| 150-200 | 9 | 165 | 123 | -41 | 67 | 10 | 167 | 131 | -36 | 53 | 10 | 167 | 116 | -50 | 65 |
| 200-250 | 6 | 218 | 130 | -88 | 93 | 6 | 220 | 150 | -70 | 72 | 6 | 220 | 129 | -91 | 101 |
| 250-300 | 3 | 261 | 194 | -67 | 73 | 4 | 262 | 188 | -75 | 78 | 4 | 262 | 172 | -91 | 92 |
| total | 107 | 94 | 135 | 41 | 86 | 97 | 112 | 136 | 23 | 65 | 97 | 112 | 122 | 9 | 69 |

Table 32. Validation results for the tropical and subtropical grasslands, savannas and shrublands biome based on spatially aggregated data of all tiers, LiDAR-based and CoFor AGB data.

| | **2010** | | | | | **2017** | | | | | **2018** | | | | |
|---|---|---|---|---|---|---|---|---|---|---|---|---|---|---|---|
| $AGB_{ref}$ bin | # cells | $AGB_{ref}$ | $AGB_{map}$ | *MD* | *RMSD* | # cells | $AGB_{ref}$ | $AGB_{map}$ | *MD* | *RMSD* | # cells | $AGB_{ref}$ | $AGB_{map}$ | *MD* | *RMSD* |
| [Mg/ha] | count | ------------------[Mg/ha] ----------------- | | | | count | --------------------[Mg/ha] ---------------- | | | | count | -------------------[Mg/ha] -------------- | | | |
| 0-50 | 191 | 27 | 44 | 17 | 41 | 70 | 26 | 30 | 4 | 36 | 66 | 26 | 29 | 3 | 37 |
| 50-100 | 96 | 70 | 65 | -5 | 43 | 62 | 68 | 48 | -20 | 32 | 64 | 68 | 47 | -21 | 33 |
| 100-150 | 20 | 123 | 113 | -11 | 58 | 21 | 124 | 117 | -7 | 48 | 20 | 124 | 109 | -15 | 48 |
| 150-200 | 31 | 182 | 215 | 33 | 73 | 14 | 178 | 198 | 20 | 72 | 13 | 179 | 202 | 23 | 69 |
| 200-250 | 70 | 226 | 227 | 1 | 59 | 52 | 229 | 243 | 14 | 67 | 50 | 231 | 241 | 10 | 66 |
| 250-300 | 82 | 274 | 245 | -28 | 50 | 76 | 274 | 242 | -33 | 64 | 77 | 276 | 239 | -37 | 66 |
| 300-400 | 60 | 326 | 250 | -76 | 89 | 83 | 332 | 256 | -77 | 91 | 84 | 334 | 250 | -84 | 97 |
| >400 | 5 | 445 | 236 | -209 | 213 | 3 | 470 | 256 | -214 | 226 | 4 | 456 | 254 | -202 | 211 |
| total | 555 | 144 | 137 | -8 | 58 | 381 | 191 | 166 | -25 | 66 | 378 | 194 | 164 | -30 | 69 |

Table 33. Validation results for the Tropical and subtropical moist broadleaf forest biome based on spatially aggregated data of all tiers, LiDAR-based and CoFor AGB data.

| | 2010 | | | | | 2017 | | | | | 2018 | | | | |
|---|---|---|---|---|---|---|---|---|---|---|---|---|---|---|---|
| $AGB_{ref}$ bin [Mg/ha] | # cells count | $AGB_{ref}$ | $AGB_{map}$ | *MD* | *RMSD* | # cells count | $AGB_{ref}$ | $AGB_{map}$ | *MD* | *RMSD* | # cells count | $AGB_{ref}$ | $AGB_{map}$ | *MD* | *RMSD* |
| | | [Mg/ha] | | | | | [Mg/ha] | | | | | [Mg/ha] | | | |
| 0-50 | 29 | 28 | 60 | 32 | 61 | 18 | 29 | 42 | 13 | 29 | 17 | 29 | 42 | 13 | 28 |
| 50-100 | 37 | 75 | 89 | 14 | 61 | 28 | 75 | 70 | -5 | 29 | 29 | 75 | 70 | -4 | 29 |
| 100-150 | 50 | 124 | 120 | -4 | 59 | 51 | 128 | 147 | 19 | 54 | 51 | 128 | 130 | 2 | 48 |
| 150-200 | 42 | 175 | 184 | 9 | 77 | 33 | 177 | 203 | 26 | 85 | 33 | 177 | 198 | 21 | 98 |
| 200-250 | 91 | 228 | 248 | 20 | 54 | 53 | 228 | 235 | 7 | 61 | 52 | 228 | 233 | 4 | 62 |
| 250-300 | 136 | 276 | 258 | -18 | 46 | 74 | 275 | 256 | -19 | 44 | 69 | 275 | 253 | -22 | 44 |
| 300-400 | 238 | 344 | 260 | -84 | 95 | 74 | 342 | 260 | -82 | 94 | 60 | 334 | 258 | -76 | 93 |
| >400 | 36 | 432 | 261 | -171 | 176 | 11 | 448 | 251 | -197 | 210 | 5 | 449 | 238 | -211 | 236 |
| total | 659 | 262 | 224 | -38 | 82 | 342 | 227 | 206 | -22 | 75 | 316 | 216 | 197 | -19 | 71 |

Table 34. Validation results for the tundra biome based on spatially aggregated data of all tiers, LiDAR-based and CoFor AGB data.

| | 2010 | | | | | 2017 | | | | | 2018 | | | | |
|---|---|---|---|---|---|---|---|---|---|---|---|---|---|---|---|
| $AGB_{ref}$ bin [Mg/ha] | # cells count | $AGB_{ref}$ | $AGB_{map}$ | *MD* | *RMSD* | # cells count | $AGB_{ref}$ | $AGB_{map}$ | *MD* | *RMSD* | # cells count | $AGB_{ref}$ | $AGB_{map}$ | *MD* | *RMSD* |
| | | [Mg/ha] | | | | | [Mg/ha] | | | | | [Mg/ha] | | | |
| 0-50 | 72 | 32 | 53 | 21 | 28 | 58 | 34 | 47 | 13 | 19 | 58 | 34 | 45 | 11 | 18 |
| 50-100 | 34 | 71 | 68 | -3 | 25 | 44 | 67 | 60 | -7 | 20 | 44 | 67 | 59 | -8 | 21 |
| 100-150 | 6 | 115 | 81 | -35 | 59 | 10 | 115 | 61 | -55 | 66 | 10 | 115 | 59 | -57 | 67 |
| total | 112 | 48 | 59 | 11 | 29 | 112 | 54 | 54 | -1 | 27 | 112 | 54 | 52 | -2 | 27 |